



NAVAL POSTGRADUATE SCHOOL  
Monterey, California



THESIS

OPTIMIZATION AND PERFORMANCE ANALYSIS OF A  
SUPERSONIC CONICAL-FLOW WAVERIDER FOR A DECK-  
LAUNCHED INTERCEPT MISSION

by

DAVID R. PRICE

June 1993

Thesis Advisor:

C. F. NEWBERRY

Co-Advisor:

J. V. BOWLES

Approved for public release; distribution is unlimited.

93-27041



93 11 4 215

# REPORT DOCUMENTATION PAGE

Form Approved

OMB No 0704-0188

Public reporting burden for this collection of information is estimated to average 1 hour per response, including the time for reviewing instructions, searching existing data sources, gathering and maintaining the data needed, and completing and reviewing the collection of information. Send comments regarding this burden estimate or any other aspect of this collection of information, including suggestions for reducing this burden, to Washington Headquarters Services, Directorate for Information Operations and Reports, 1215 Jefferson Davis Highway, Suite 1204, Arlington, VA 22202-4302, and to the Office of Management and Budget, Paperwork Reduction Project (0704-0188), Washington, DC 20503.

1. AGENCY USE ONLY (Leave blank)

2. REPORT DATE

11 June 1993

3. REPORT TYPE AND DATES COVERED

Master's Thesis

4. TITLE AND SUBTITLE

OPTIMIZATION AND PERFORMANCE ANALYSIS OF A SUPERSONIC CONICAL-FLOW WAYERIDER FOR A DECK-LAUNCHED INTERCEPT MISSION

5. FUNDING NUMBERS

6. AUTHOR(S)

Price, David R.

7. PERFORMING ORGANIZATION NAME(S) AND ADDRESS(ES)

Naval Postgraduate School  
Monterey, CA 93943-5000

8. PERFORMING ORGANIZATION  
REPORT NUMBER

9. SPONSORING / MONITORING AGENCY NAME(S) AND ADDRESS(ES)

10. SPONSORING / MONITORING  
AGENCY REPORT NUMBER

11. SUPPLEMENTARY NOTES

The views expressed in this thesis are those of the author and do not reflect the official policy or position of the Department of Defense or the U.S. Government.

12a. DISTRIBUTION / AVAILABILITY STATEMENT

Approved for public release, distribution is unlimited.

12b. DISTRIBUTION CODE

13. ABSTRACT (Maximum 200 words)

An aircraft configuration for a deck launched intercept mission was investigated as part of an on-going waverider study by the Naval Postgraduate School and the NASA Ames Research Center. The mission requirements for the carrier-launched and recovered aircraft included Mach 6 cruise out to a 1000 nautical mile combat radius and 20 minutes of combat followed by return to the carrier. A conical-flow waverider served as the starting point for the aircraft configuration. A hydrocarbon scramjet was integrated with the waverider body. The aft end of the waverider was faired to decrease the base area thereby reducing the transonic base drag. A numerical optimization was then completed to maximize the product of L/D (lift to drag ratio) and  $I_{sp}$  (specific impulse). Variables for the optimization included the cone shock angle (used to derive the conical flow waverider) and the geometry of both the waverider body and the integrated propulsion system. The vehicle was constrained to a minimum volume of 3240 cubic feet, a maximum span of 60 feet and a fixed length of 60 feet. The integrated propulsion system was constrained to produce a minimum contraction ratio of 12.0 and assurance that the cowl shock was within an acceptable distance of the inlet shoulder of the combustor. The optimum configuration met or exceeded all constraints. L/D comparisons were made between the integrated configuration (i.e., the subject of this study), pure Mach 6 optimized waveriders and historical trends. Additionally, model design, test media and test parameter selection were studied for planned low speed wind and water tunnel tests as well as performance predictions for the planned wind tunnel tests.

14. SUBJECT TERMS

Waveriders, Hypersonics, Aircraft Design

15. NUMBER OF PAGES

82

16. PRICE CODE

17. SECURITY CLASSIFICATION  
OF REPORT

UNCLASSIFIED

18. SECURITY CLASSIFICATION  
OF THIS PAGE

UNCLASSIFIED

19. SECURITY CLASSIFICATION  
OF ABSTRACT

UNCLASSIFIED

20. LIMITATION OF ABSTRACT

UL

Approved for public release; distribution is unlimited.

Optimization and Performance analysis of a Supersonic Conical-Flow Waverider for a Deck-Launched Intercept Mission

by

David R. Price  
Lieutenant, United States Navy  
B. S., United States Naval Academy, 1985

Submitted in partial fulfillment  
of the requirements for the degree of

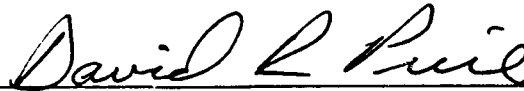
MASTER OF SCIENCE IN ASTRONAUTICAL ENGINEERING

from the

NAVAL POSTGRADUATE SCHOOL

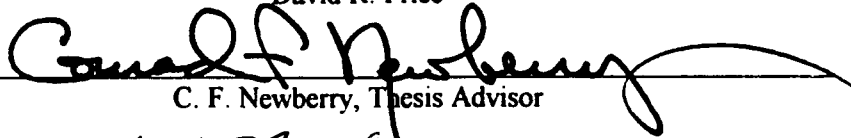
June 1993

Author:

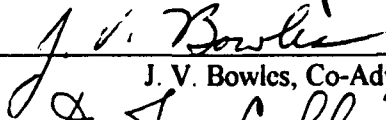


David R. Price

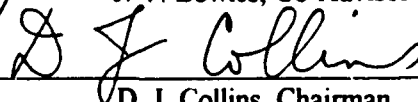
Approved By:



C. F. Newberry, Thesis Advisor



J. V. Bowles, Co-Advisor



D. J. Collins, Chairman

Department of Aeronautics and Astronautics

## ABSTRACT

An aircraft configuration for a dock launched intercept mission was investigated as part of an on-going waverider study by the Naval Postgraduate School and the NASA Ames Research Center. The mission requirements for the carrier-launched and recovered aircraft included Mach 6 cruise out to a 1000 nautical mile combat radius and 20 minutes of combat followed by return to the carrier. A conical-flow waverider served as the starting point for the aircraft configuration. A hydrocarbon scramjet was integrated with the waverider body. The aft end of the waverider was faired to decrease the base area thereby reducing the transonic base drag. A numerical optimization was then completed to maximize the product of  $L/D$  (lift to drag ratio) and  $I_{sp}$  (specific impulse). Variables for the optimization included the cone shock angle (used to derive the conical flow waverider) and the geometry of both the waverider body and the integrated propulsion system. The vehicle was constrained to a minimum volume of 3240 cubic feet, a maximum span of 60 feet and a fixed length of 60 feet. The integrated propulsion system was constrained to produce a minimum contraction ratio of 12.0 and assurance that the cowl shock was within an acceptable distance of the inlet shoulder of the combustor. The optimum configuration met or exceeded all constraints.  $L/D$  comparisons were made between the integrated configuration (i.e., the subject of this study), pure Mach 6 optimized waveriders and historical trends. Additionally, model design, test media and test parameter selection were studied for planned low speed wind and water tunnel tests as well as performance predictions for the planned wind tunnel tests.

DTIC COPY AVAILABLE FROM 3

Accession For	
NTIS CRA&I	<input checked="" type="checkbox"/>
DTIC TAB	<input type="checkbox"/>
Unannounced	<input type="checkbox"/>
Justification	
By	
Distribution /	
Availability Codes	
Dist	Availability or Special
<b>A-1</b>	

## TABLE OF CONTENTS

I. INTRODUCTION .....	1
A. HISTORICAL PERSPECTIVE .....	3
B. DESIGN MOTIVATION .....	4
II. MISSION DEFINITION AND ANALYSIS .....	8
A. MISSION SPECIFICS .....	8
B. AIRCRAFT SIZING .....	9
C. ENGINE AND FUEL SELECTION .....	10
III. WAVERIDER GENERATION AND OPTIMIZATION .....	12
A. WAVERIDER GENERATION .....	15
B. OPTIMIZATION .....	16
C. OPTIMIZATION METHODOLOGY .....	16
D. FIXED GEOMETRY PARAMETERS .....	19
1. Vehicle Length .....	19
2. Combustor .....	19
3. Equivalence Ratio .....	21
4. Fairing Start Point .....	22
5. Assumptions .....	22
E. OPTIMIZATION CONSTRAINTS .....	23
1. Volume .....	23
2. Span to Length Ratio .....	23
3. Contraction Ratio .....	24
4. Unaccelerated Level Flight Requirements .....	24
5. Leading Edge Temperature .....	25
6. Shock on Shoulder .....	26
F. OPTIMIZATION VARIABLES .....	27
1. Generating Curve .....	27
2. Propulsion System Geometry .....	28
3. Leading Edge Radius .....	30
4. Generating Flowfield Shock Angle .....	30
5. Fairing Start Angle .....	30
G. OBJECTIVE FUNCTION .....	30
IV. OPTIMIZATION RESULTS .....	32
A. FLOW PROPERTIES .....	32
B. OPTIMUM BODY GEOMETRY .....	33
1. Generating Shock Angle .....	33
2. Generating Curve .....	33
3. Span .....	33

4. Internal Volume .....	34
5. Leading Edge Radius .....	34
C. OPTIMUM PROPULSION SYSTEM GEOMETRY .....	36
D. OPTIMUM CONFIGURATION PERFORMANCE .....	38
E. COMPARISON WITH PRELIMINARY SIZING RESULTS .....	38
V. PERFORMANCE PREDICTION AND COMPARISONS .....	39
A. COEFFICIENT OF LIFT .....	39
B. CRUISE PERFORMANCE .....	41
C. LOW SPEED PERFORMANCE COMPARISONS .....	42
VI. TEST PREPARATION .....	46
A. WIND TUNNEL TESTS .....	46
1. Wind Tunnel Description .....	46
2. Test Parameters .....	47
B. WATER TUNNEL TESTS .....	47
C. MODEL PREPARATION .....	49
1. Wind Tunnel Model Sizing .....	49
2. Balance Selection .....	49
3. Water Tunnel Model Sizing .....	49
4. Model Material and Construction .....	49
VII. FOLLOW-ON RESEARCH .....	51
A. PLANNED NEAR-TERM TESTING .....	51
B. ADDITIONAL AREAS FOR RESEARCH .....	52
VIII. CONCLUSION .....	54
APPENDIX A - PRELIMINARY AIRCRAFT SIZING .....	55
A. WING GEOMETRY .....	55
1. Aspect Ratio .....	55
2. Wing Area .....	55
B. THRUST-TO-WEIGHT RATIO .....	55
1. Takeoff .....	55
2. Cruise .....	56
C. TAKEOFF WEIGHT ESTIMATION .....	56
1. Initial Takeoff Weight Estimate .....	57
2. Empty Weight Fraction .....	57
3. Mission Segment Weight Fractions .....	58
3. Fuel Fraction .....	63
4. Resulting First Order Estimation of Takeoff Weight .....	63
APPENDIX B - WAVERIDER CONSTRUCTION .....	64
STEP 1. SOLVE THE FLOWFIELD .....	64
STEP 2. GENERATE FREESTREAM UPPER SURFACE .....	64
STEP 3. LOWER COMPRESSION SURFACE .....	65
APPENDIX C - MODEL SIZING CALCULATIONS .....	66
A. WIND TUNNEL MODEL .....	66
B. WATER TUNNEL MODEL .....	68

REFERENCE LIST .....	70
INITIAL DISTRIBUTION LIST .....	72

## LIST OF TABLES

TABLE	PAGE
TABLE 2.1 MISSION SUMMARY .....	9
TABLE 2.2 PRELIMINARY SIZING SUMMARY .....	10
TABLE 2.3 ENGINE SIZING/PERFORMANCE SUMMARY .....	11
TABLE 3.1 COMBUSTOR FLOWFIELD ANALYSIS SUMMARY .....	15
TABLE 3.2 INLET/NOZZLE FLOWFIELD ANALYSIS SUMMARY .....	15
TABLE 3.3 SIZE COMPARISON OF CARRIER-BASED AIRCRAFT .....	19
TABLE 3.4 COMBUSTOR EXPANSION .....	20
TABLE 3.5 INJECTOR GEOMETRY .....	20
TABLE 3.6 GENERATING CURVE COEFFICIENTS .....	28
TABLE 3.7 PROPULSION SYSTEM GEOMETRY VARIABLES .....	29
TABLE 4.1 OPTIMUM CONFIGURATION FLOWFIELD SUMMARY .....	32
TABLE 4.2 GENERATING CURVE COEFFICIENTS FOR OPTIMUM CONFIGURATION .....	33
TABLE 4.3 OPTIMIZED CONFIGURATION BODY GEOMETRY .....	36
TABLE 4.4 OPTIMIZED CONFIGURATION PROPULSION SYSTEM GEOMETRY .....	36
TABLE 4.5 OPTIMIZED CONFIGURATION PERFORMANCE SUMMARY .....	38
TABLE 4.6 COMPARISON WITH PRELIMINARY SIZING .....	38
TABLE 5.1 $C_L$ VALUES FROM LOW AR THEORY AND VORLAX .....	40
TABLE 5.2 CRUISE PERFORMANCE COMPARISON .....	42
TABLE 6.1 7075 ALUMINUM PROPERTIES .....	50



## LIST OF FIGURES

FIGURE	PAGE
Figure 1.1 Breguet Ranges of Various Aircraft Types .....	3
Figure 1.2 Nonweiler's Caret Wing .....	4
Figure 1.3 Conical Flow Waverider .....	6
Figure 1.4 Bowcutt's Best Optimum Waverider at Mach 6 .....	7
Figure 1.5 Mach 6 Waverider Tested by Vanhoy .....	7
Figure 2.1 Mission Profile .....	9
Figure 3.1 Design Process .....	14
Figure 3.2 Optimization Flowchart .....	18
Figure 3.3 Fixed Combustor Geometry .....	20
Figure 3.4 Pessin's Fairing Geometry .....	23
Figure 3.5 Contraction Ratio Geometry .....	24
Figure 3.6 Forces Acting During Level Unaccelerated Cruise .....	26
Figure 3.7 Shock on Ramp Geometry .....	27
Figure 3.8 Generating Curve Geometry (Aft View) .....	28
Figure 3.9 Propulsion System Geometry .....	29
Figure 4.1 Resulting Optimum Configuration .....	35
Figure 4.2 Optimized Configuration Propulsion System Geometry .....	37
Figure 5.1 $C_L$ vs $\alpha$ .....	41
Figure 5.2 Hypersonic Configuration Performance Comparison .....	43
Figure 5.3 Results for a Series of Optimized Mach 6 Waveriders from the University of Maryland .....	44
Figure 5.4 $C_L$ Comparisons .....	45
Figure 6.1 Planned Installation of Optimized Hydrocarbon-Powered Waverider in NPS 32x45 inch Wind Tunnel .....	47
Figure 6.2 The NPS Flow Visualization Water Tunnel Facility .....	48
Figure 7.1 Hydrocarbon-Powered Waverider Aircraft Configuration .....	53
Figure A.1 Catapult End Speeds .....	57
Figure A.2 Arresting Gear Weight Limits .....	58
Figure A.3 Specific Impulse Trends .....	61
Figure B.1 Construction of General Cone-Derived Waverider .....	65

## ACKNOWLEDGMENTS

My sincerest appreciation goes to my advisors, Prof. Conrad F. Newberry, Naval Postgraduate School, and Mr. Jeffrey V. Bowles, NASA Ames Research Center, for their incredible and flexible support for what has been a most dynamic research project. They have been central to turning a few ideas for a possible waverider mission into a full-blown concept exploration. They have given me insights and experience in real world engineering far beyond what any graduate student could hope for. Thanks to all the exceptionally talented people at the Systems Analysis Branch, NASA Ames Research Center who provided support for this project. They represent an irreplaceable national resource. Specifically, thanks to Loc Huynh for working so hard and solving the many problems we encountered during the optimizations and for sharing his knowledge of everything from basic aerodynamics to optimization theory. Thanks to Tom Whitaker for bringing me up to speed on the computers and for breathing life into the waveriders with his incredible computer graphics simulations, and to J. R. for his work on the VORLAX code. I was constantly amused and amazed by the great things that came out of their office. Also, thanks to Mr. George Kidwell, Branch Chief, for allowing his folks to give their time and talent to this project. Finally, my greatest appreciation goes to my wonderful wife, Susan, and my sons, Sean and Nick, for their patience, understanding and support throughout this project. Without their help it would not have been possible. Thanks.

David Price, June 1993

Monterey, California

## I. INTRODUCTION

The quest for speed has been a continuous theme in aeronautical history. The reasons for this quest have been many and varied; not the least of which has been the pure thrill and excitement of doing something in the present that could not be done in the past. Engineers, manufacturers, pilots and spectators have all shared in the excitement of increasing aircraft performance. Of course, the excitement of going faster does not, in itself, justify the cost. As noted by Kuchemann, there is a social aspect of aircraft design to consider [Ref. 1:p. 3]. Going faster must have a value to society which justifies the cost. Increases in speed have historically been worthwhile because they increased the convenience and decreased the time to travel a given distance, thereby increasing society's productivity. An increase in any figure-of-merit of aircraft performance must be balanced by other factors, such as productivity, cost, safety and environmental issues, in order to determine whether or not the increase is worthwhile.

Kuchemann envisioned the peaceful future of our planet as a "global village" wherein which people could reach all of the world's major population centers from any location in only a few hours. Kuchemann argued that this reduction in travel time was necessary to overcome the reluctance of people to travel great distances and that bringing about this "global village" by reducing travel times should be one of the social goals of aviation. Increasing the speed of aircraft may be the only way to achieve Kuchemann's vision. From our present status in aviation, hypersonic flight is the next logical step in the aircraft velocity spectrum. One possibility for efficient hypersonic flight is waverider configurations. [Ref. 1:pp. 448-451]

To achieve his "global village", Kuchemann stated that transport aircraft of the future should be capable of traveling a "global range" (half the earth's circumference) in two hours. To this end, he defined a figure-of-merit by which to compare various aircraft types, as the fraction of the "global range" an aircraft was capable of traveling in two hours. Figure 1.1 shows a graphical representation of Kuchemann's comparison.  $R/R_g$  represents the fraction of the "global range" achievable in two hours by the different types of aircraft. Three general aircraft types are considered; swept, slender and waveriders. The aircraft type is basically defined by its span to length ratio,  $s/l$ , cruise Mach number,  $M_0$ , and body/wing shape; swept, slender or waverider. Three additional lines of interest subdividing the figure are the  $M_0=1$  line, the  $s/l=0.2$  line and the  $\beta s/l=1$  line. Span to length of less than 0.2 leads to aircraft generally inadequate on the airfield [Ref. 1:p. 449].  $\beta s/l=1$  is where delta wings have a "nominally sonic leading edge." The figure shows that waveriders are best suited for the task of bringing the time for traveling "global range" down to a few hours. [Ref. 1:pp. 448-451]

Waverider technology has a wide range of possible applications, including, but not limited to, the well-publicized hypersonic transports of the future. The L/D performance of waveriders makes them a logical starting point for improving the performance of Maneuvering Reentry Vehicles (MaRV) and extending the range of Hypersonic Glide Vehicles (HGV) [Ref. 2:pp. 1-5]. Waverider characteristics also lend themselves to several space applications such as aero-assisted plane changes or orbit modifications and atmospheric long range cruising planetary probes [Ref. 3:p. 9]. Additionally, waveriders show promise as baseline configurations for single-stage-to-orbit vehicles. Their potentially superior L/D performance when operating at design Mach number compared to conventional wing/body configurations makes waveriders logical candidates for the next generation of hypersonic aircraft.

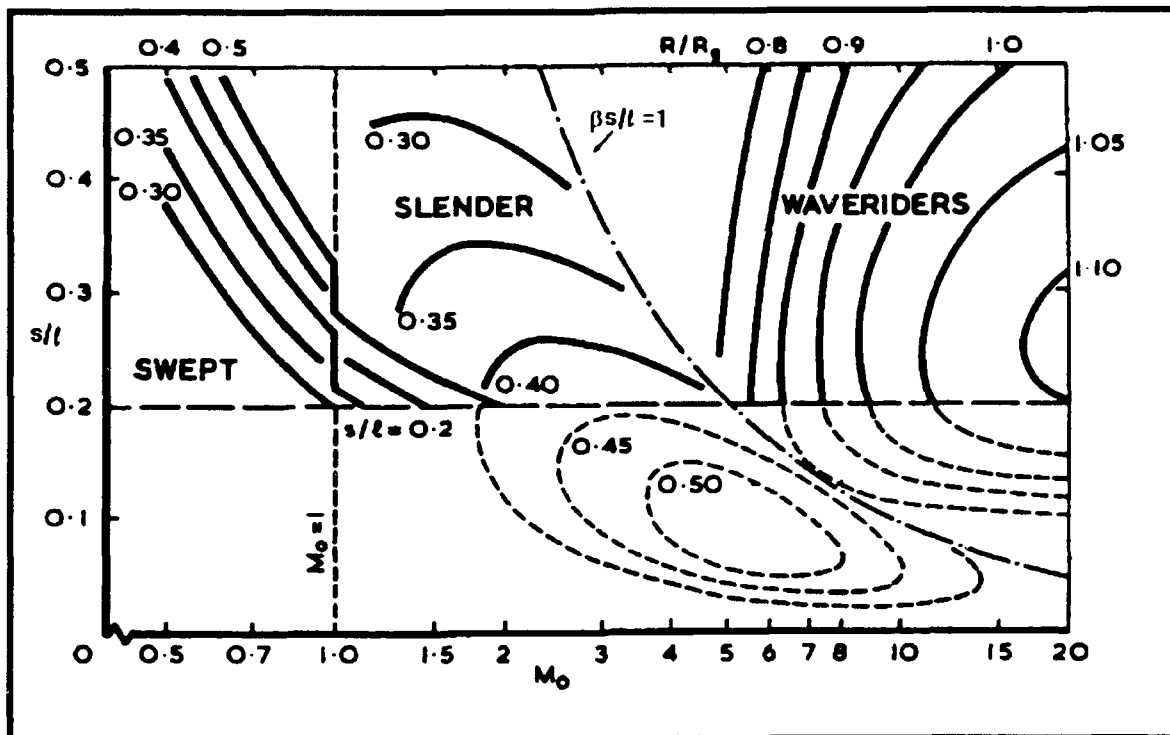


Figure 1.1 Breguet Ranges of Various Aircraft Types. From Ref. 1.

## A. HISTORICAL PERSPECTIVE

The history of waveriders apparently began in 1959 when Nonweiler introduced the idea of a three dimensional body derived from the flowfield behind a planar shock [Ref. 4:pp. 521-528]. This first waverider had a delta planform and a caret shaped cross section. When flying at the design Mach number, the shock is attached to the leading edges preventing spanwise flow and spillage from the lower to upper surface. The high pressure flow behind the shock is captured between the shock and the lower surface of the body resulting in increased lift. Figure 1.2 shows Nonweiler's caret wing.

In the 1960's, 1970's and 1980's, the design of waveriders was extended to include those derived from other known flowfields such as caused by right circular and elliptic cones. Figure 1.3 shows a conical flow waverider. In the late 1980's, Bowcutt and Anderson continued the progress in waverider development with viscous optimized

waveriders designed to maximize  $L/D$ . Figure 1.4 shows the Bowcutt/Anderson optimum result for a Mach 6 waverider design. [Ref. 6: pp. 15-19]

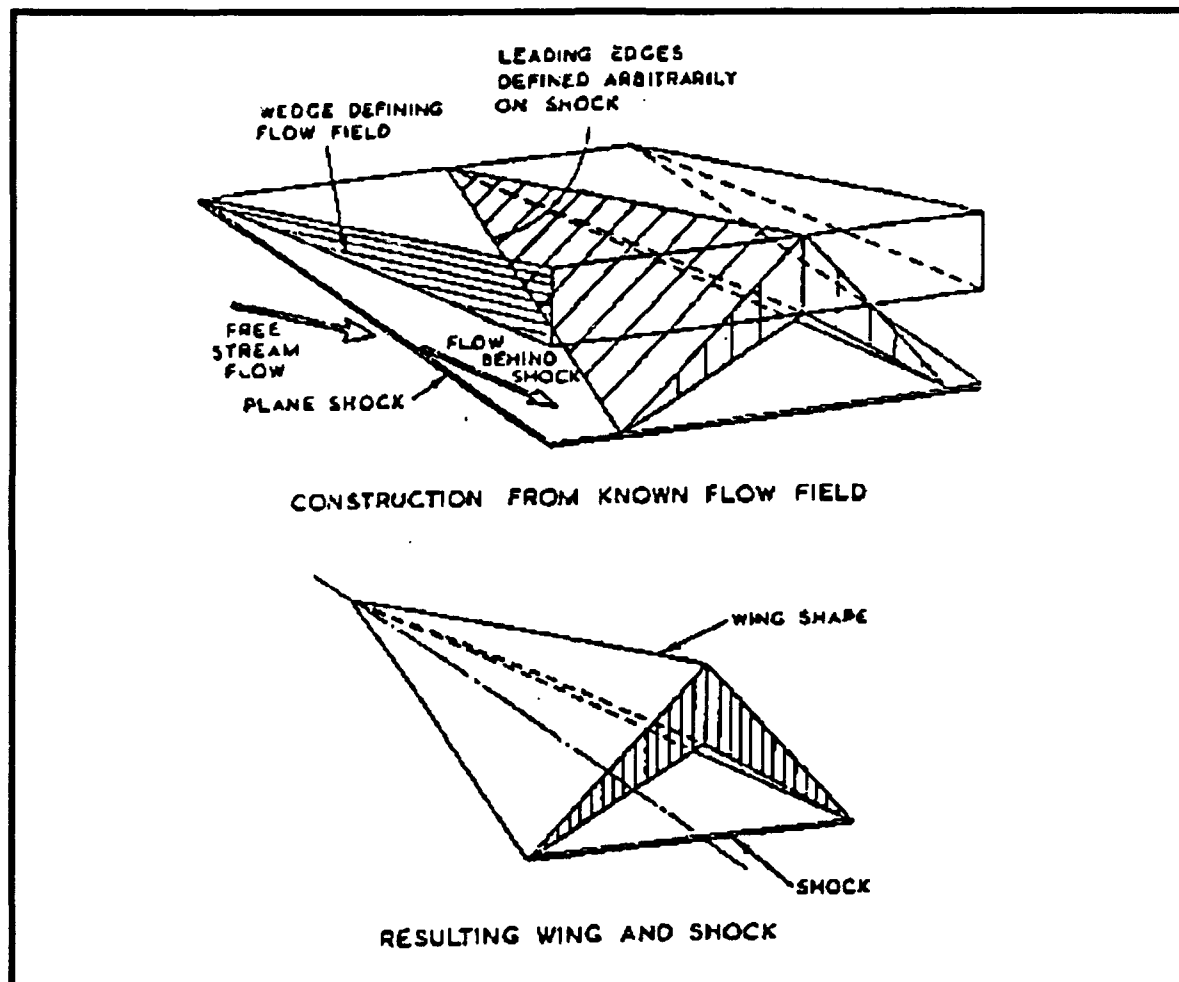


Figure 1.2 Nonweiler's Caret Wing. From Ref. 5.

## B. DESIGN MOTIVATION

The configuration studied herein seeks to provide one possibility in the next logical step in waverider evolution; the design and optimization of a mission-specific waverider.

As Schindel [Ref. 7] points out, optimum waveriders are not feasible vehicles due to several practical considerations. These include volume requirements, the effects of base drag and the practicality of the proposed vehicle shape (construction and internal packing requirements). Additionally, an actual vehicle based on a waverider must be designed as an integrated engine/airframe unit. [Ref. 7:p. 1]

In 1988 Vanhoy [Ref. 8] expanded the work of Bowcutt into the low-speed regime with wind tunnel tests of a Mach 6 viscous optimized waverider. Figure 1.5 shows the waverider used in Vanhoy's tests. In selecting the geometry for his tests, Vanhoy had to address such concerns as the ease of construction of the selected shape and whether the base thickness was adequate for use with a sting mount [Ref. 8:p. 8]. Such constraints represent only initial considerations in trying to create an actual vehicle from a waverider. The project described herein considers mission and performance constraints on the full scale vehicle as well as the requirements of a low-speed wind tunnel model.

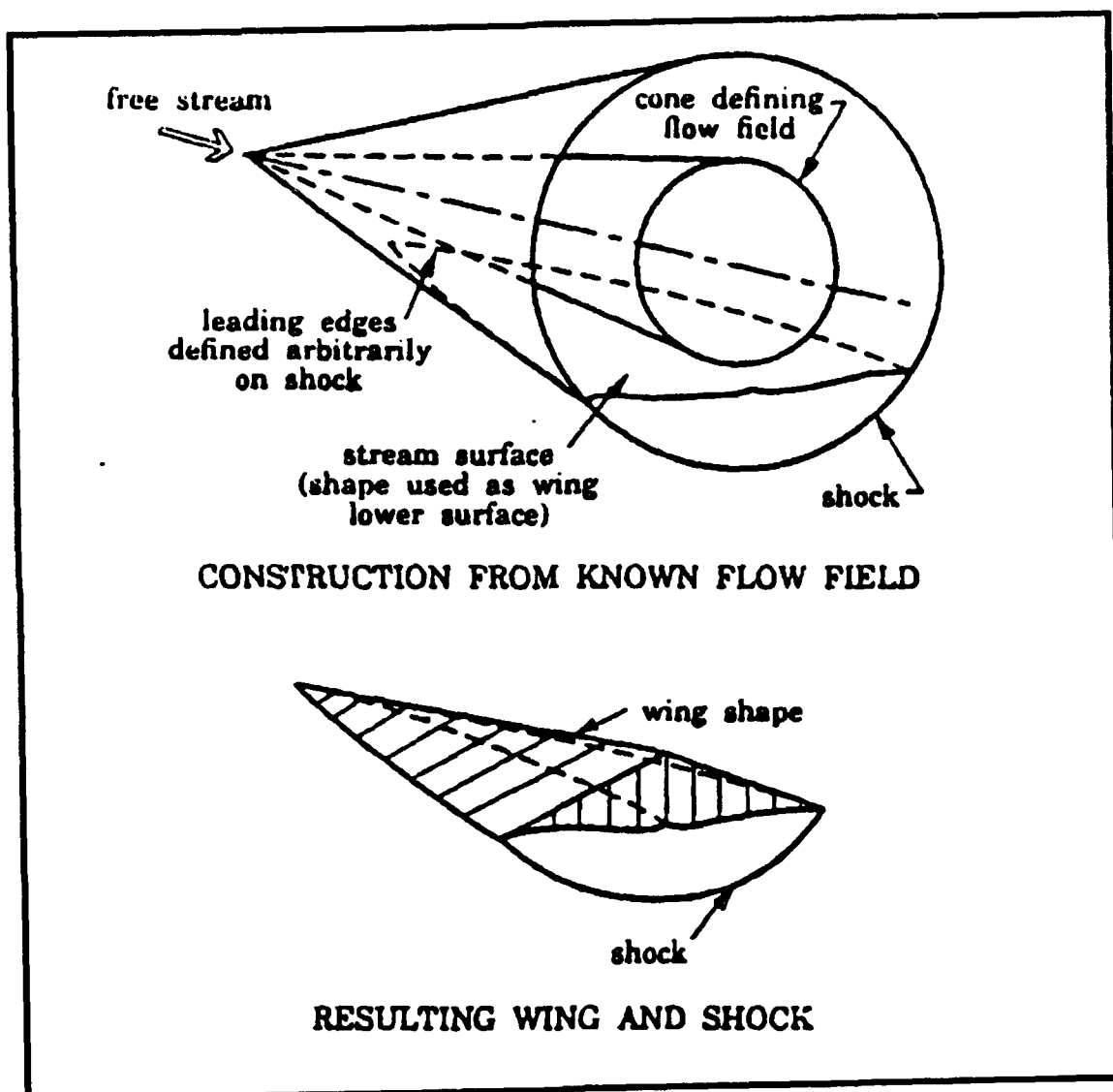


Figure 1.3 Conical Flow Waverider. From Ref. 5.



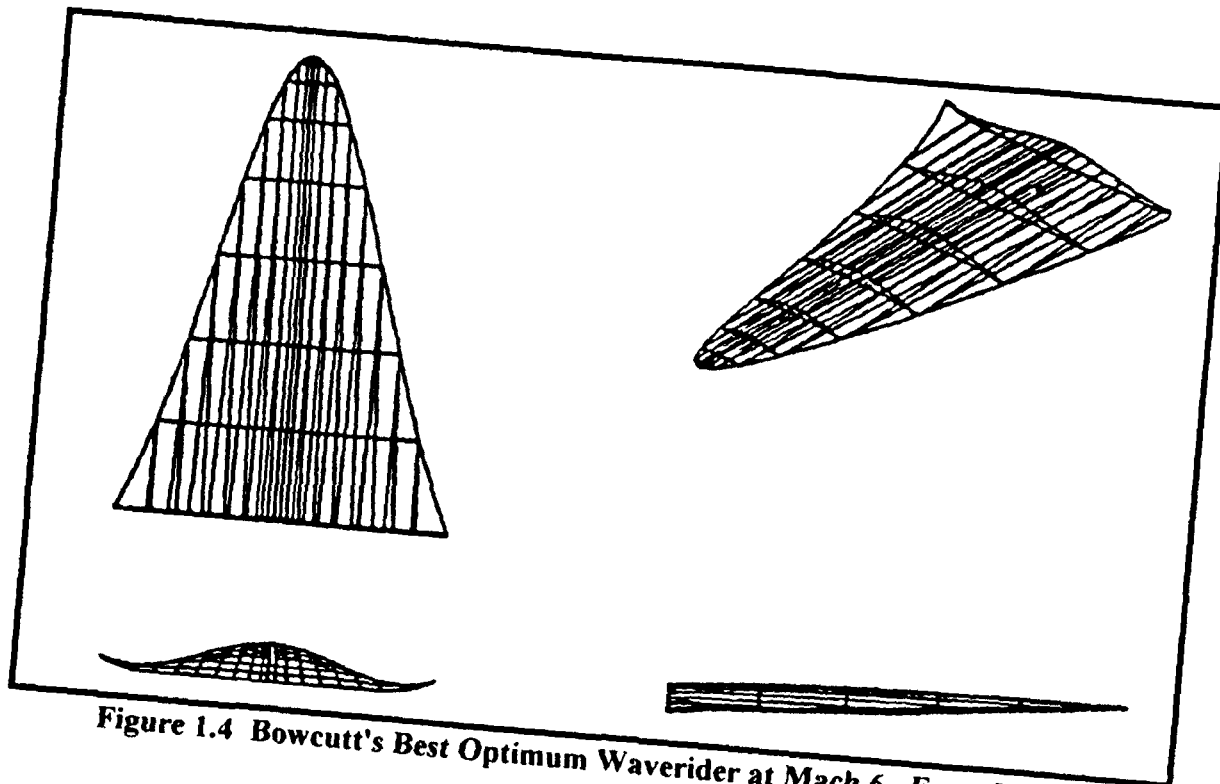


Figure 1.4 Bowcutt's Best Optimum Waverider at Mach 6. From Ref. 6.

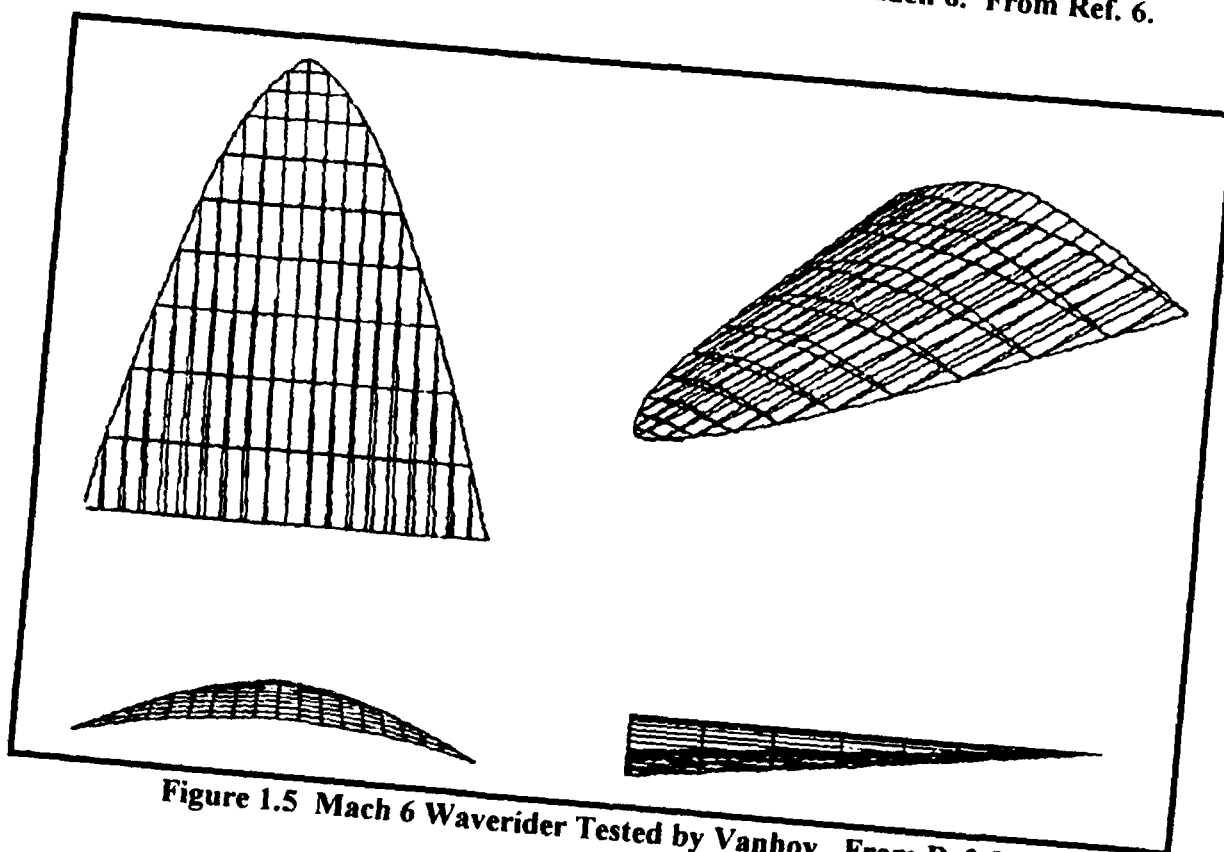


Figure 1.5 Mach 6 Waverider Tested by Vanhoy. From Ref. 8.

## II. MISSION DEFINITION AND ANALYSIS

The carrier-launched intercept mission was specifically chosen for the development of the waverider design discussed herein. Waveriders seem well suited to this type mission due to their inherent advantage in low drag at hypersonic speeds. Speed is an important factor in intercept missions because it translates into distance away from what the interceptor is protecting. Waveriders may also bring a better than average maneuverability at hypersonic speeds to the mission.

### A. MISSION SPECIFICS

Building on the SR-71 and X-15 design, production and operations databases, a Mach number of six was chosen for the cruise speed as a logical, practical and technically feasible step up from current capabilities. *Carrier basing imposes additional design constraints, including takeoff and landing speeds and weights, length and span and fuel type.* It was decided that the more restrictive constraints of carrier operation during the initial design phase would lead to greater flexibility in relaxing constraints, if at a later date a similar land-based mission were desired. For example, design constraints such as length and weight might be relaxed for a land-based waverider. Figure 2.1 depicts the proposed waverider intercept mission. Table 2.1 contains specific mission parameters chosen for this design.

**TABLE 2.1**  
**MISSION SUMMARY**

Range	1000 nautical mile combat radius
Cruise	Mach 6 at Best Cruise Altitude (BCA)
Combat	Twenty minutes on-station; airborne intercept, no dogfighting
Loiter	Twenty minutes at sea level at Best Loiter Speed (BLS)
Approach Speed	$\leq 140$ KTS
Takeoff and Landing	Catapult launch and arrested recovery

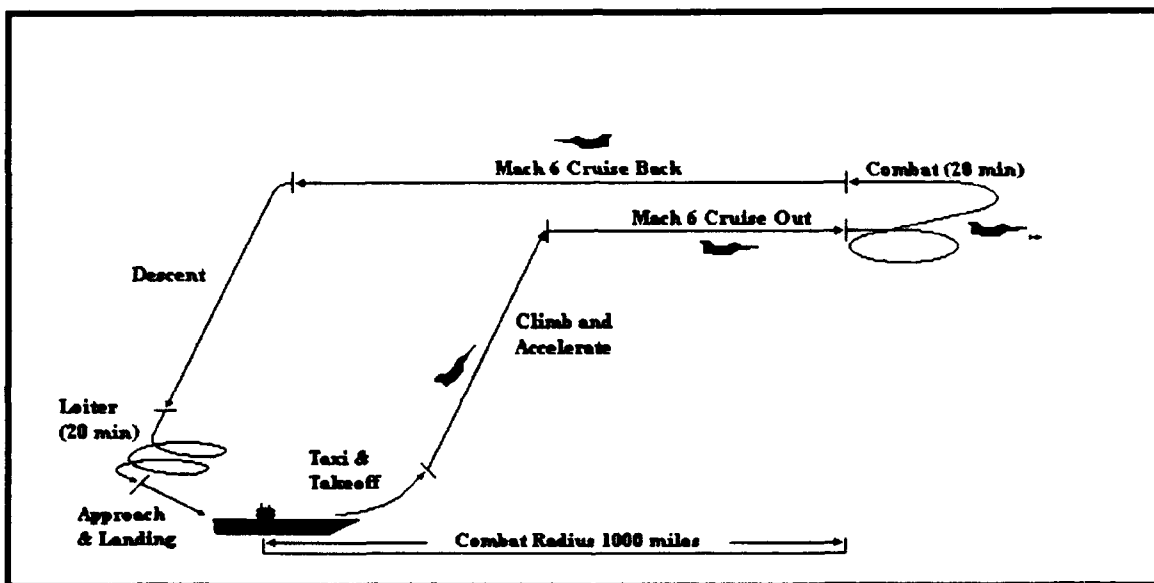


**Figure 2.1 Mission Profile.**

## **B. AIRCRAFT SIZING**

An aircraft sizing study was completed for the selected mission parameters to be used herein for baseline comparison. The sizing was based on historical trends following Nicolai [Ref. 9] and Raymer [Ref. 10]. It is important to note that the sizing studies performed for this project are based on existing historical and current data bases. The lack of data on hypersonic aircraft makes predictions of aircraft size requirements and performance only somewhat better than an educated guess. It is, however, important in

helping to validate conceptual results. Sizing began with weight, length and span limitations imposed by carrier basing. The sizing calculations are contained in Appendix A. A summary of preliminary sizing assumptions and results for the mission delineated above are given in Table 2.2. A comparison of preliminary sizing results with the optimized configuration is made in Section IV.

**TABLE 2.2**  
**PRELIMINARY SIZING SUMMARY**

Length	60 feet
Span	60 feet
Aspect Ratio	1.35
Wing Area	2670 square feet
Maximum takeoff gross weight	100,000 pounds
Maximum landing weight	50,000 pounds
Empty weight fraction	0.42

### **C. ENGINE AND FUEL SELECTION**

For Mach 6 cruise, a supersonic combustion ramjet (scramjet) was selected as the appropriate propulsion system. Hypersonic aircraft require a more careful integration of the aircraft engine and body than conventional subsonic and supersonic aircraft due to their use of the aircraft body as compression and expansion surfaces for the engine. For the waveriders studied, the engine and body were designed from the beginning to work together as a single unit. Compression for the propulsion system is "mixed" in that it is accomplished by both internal and external means. External compression is accomplished by a series of oblique shocks which are created by ramps on the lower forebody. Internal compression is accomplished by a final oblique shock generated by the leading edge of the engine cowl. For flight below about Mach 3 the scramjet is impractical and the use of more conventional engines becomes necessary. It is envisioned that two turbojets similar to J-58s could be used for takeoff, landing and low speed flight. For a 100,000 pound

aircraft this turbojet propulsion system would provide a thrust to weight ratio at takeoff of approximately 0.6. A longtime requirement of two engines for carrier-based aircraft has been standard practice in the U. S. Navy and is used in the mission analysis and sizing studies for this project. Table 2.3 contains a summary of engine sizing and performance.

The two primary fuels considered for this design were hydrogen and ethylene. Ethylene,  $C_2H_4$ , was chosen as the fuel for this design for several reasons. One of the primary concerns for fuel selection was shipboard handling. Another major factor considered was the low density and therefore higher volume requirements of hydrogen. This creates problems for both storage space onboard ship and increased aircraft internal volume requirements to fly the same mission. Existing size constraints for carrier-based aircraft would limit the range of a hydrogen powered waverider. Finally, ethylene is very similar to JP-7; the fuel used by current J-58 turbojets. This allows the entire flight to be flown using a single fuel.

**TABLE 2.3**  
**ENGINE SIZING/PERFORMANCE SUMMARY**

Required T/W (takeoff)	0.55-0.8
Required T/W (cruise)	0.25
Specific Impulse (hydrocarbon scramjet)	1300 seconds
J58 Max takeoff thrust (sea level)	30,000 pounds

### III. WAVERIDER GENERATION AND OPTIMIZATION

The waveriders analyzed for this project were generated using the Waverider Code developed by the Systems Analysis Branch at the NASA Ames Research Center. The Waverider Code and its subroutines are a subset of the Hypersonic Aircraft Vehicle Optimization Code (HAVOC), also created by the Systems Analysis Branch. The computer used was a Silicon Graphics Iris workstation. The design goal of this project was to achieve a hydrocarbon-scamjet-powered waverider optimized for mission performance, while keeping computer processing time to a minimum and checking the results enroute to solving for the optimum configuration.

Due to the much increased computer processing time of the nose-to-tail flow solution by the Waverider Code when using hydrocarbon fuels (vice hydrogen), it was decided to begin by optimizing pure waveriders and then hydrogen-powered waveriders to generate a starting point for a hydrocarbon-powered waverider optimization. A non-optimized waverider had to be generated which met the optimization constraints to be used as a starting point for optimization due to difficulties experienced by the optimization routine when starting outside the defined constraints. This was accomplished by generating over one hundred waveriders to develop an understanding of how each variable affected the final waverider geometry and then finally moving toward a set of design parameters that produced a waverider which met the desired constraints.

To save computer processing time and be able to more quickly determine an optimized waverider's suitability, it was decided to begin by optimizing a "pure" waverider (no engine, no base fairing) for maximum  $L/D$ . The result of this optimization would in turn be used as the initial geometry for a waverider with a base fairing, optimized for maximum

L/D. The resulting optimized, faired waverider was used as the starting point for optimizing a hydrogen-scramjet-powered waverider. The objective function for this powered waverider was changed from L/D to the product of L/D and  $I_{sp}$ . Using the product of L/D and  $I_{sp}$  resulted in tradeoffs during the optimization process between aerodynamic and engine performance. Finally, the result of this optimization was used as the starting point for a hydrocarbon-scramjet-powered waverider optimized to maximize the product of L/D and  $I_{sp}$ . Figure 3.1 illustrates the design process used.

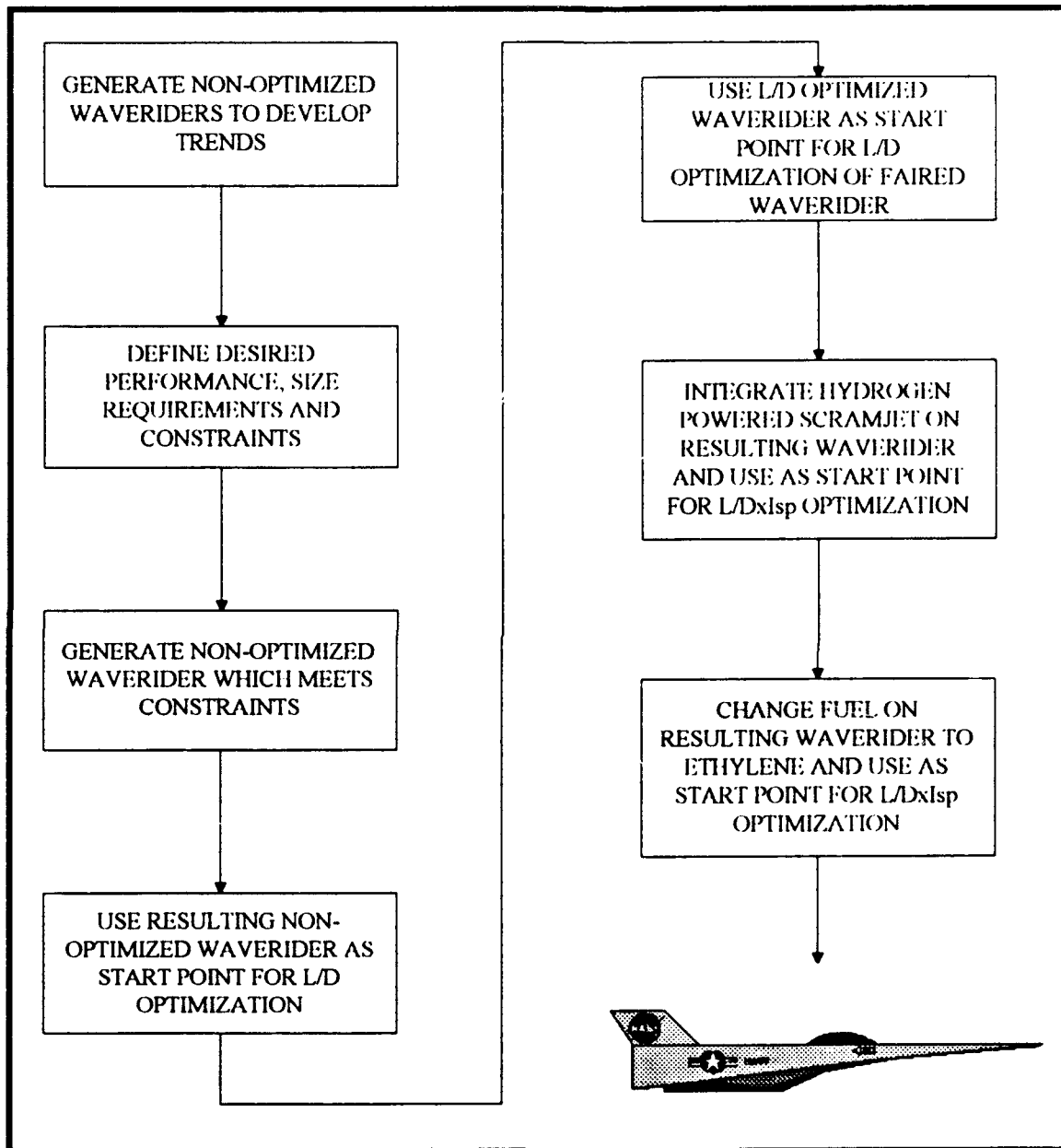


**Figure 3.1 Design Process.**



## A. WAVERIDER GENERATION

The Ames Waverider Code begins its computations by constructing a general cone-derived waverider from a user-defined flowfield as explained in Appendix B. It departs from the resulting "pure" waverider with the addition of an integrated forebody ramp system, scramjet engine and nozzle. At the discretion of the designer, the lower surface is faired at the aft end to reduce the area of the base and thereby decrease the base drag at low supersonic and transonic speeds. The program then computes a nose to tail solution of the conical flowfield under the vehicle by solving the Taylor - Maccoll equation for conical flow. The code creates a data file which defines the geometry. This file is stored for later use to generate a three dimensional visualization of the body.

The "nose to tail" solution of the conical flowfield includes a 2-D analysis of the inlet and nozzle flowfield and a quasi 1-D analysis inside the combustor. Both analyses consider real gas effects. Table 3.1 and 3.2 list highlights of each.

**TABLE 3.1  
COMBUSTOR FLOWFIELD ANALYSIS SUMMARY**

Quasi 1-D Analysis
Hydrogen and Hydrocarbon Fuels (or mixtures)
Multiple injector stations (Mixing model - Combustor Efficiency)
Augmented Pre-burning capability
Heat balanced
- Ramp/Nozzle heat transfer rate input vs. Mach no.
- Combustor skin friction coefficient input vs. Mach no.

**TABLE 3.2  
INLET/NOZZLE FLOWFIELD ANALYSIS SUMMARY**

2-D planar, inviscid analysis
Real gas, equilibrium or frozen flow in nozzle with mass fraction specified
Ramp/Cowl geometry input as a function of Mach no.
Oblique shocks, isentropic waves and sliplines (contact surfaces) computed

## B. OPTIMIZATION

A numerical optimization was achieved using VMA Engineering's Design Optimization Tools (DOT). DOT is an optimization routine which varies user-selected parameters to find the local maximum or minimum value of a selected design objective function (i.e.,  $L/D$  or  $L/D \cdot I_{sp}$ ) while satisfying multiple user-defined constraints. It uses finite difference methods to calculate the gradients of the objective and constraint functions. DOT solves this nonlinear optimization problem iteratively.

Specifically, DOT uses the Sequential Linear Programming Method to implement the Modified Method of Feasible Directions algorithm and find an optimum solution (in this case one which maximized  $L/D \cdot I_{sp}$  while still meeting all of the constraints). This method creates a Taylor series to approximate the objective and constraint functions and uses the resulting approximation for optimization, instead of the original nonlinear functions. This allows for easier calculation of the objective and constraint functions during the optimization. Additionally, the objective and constraint gradients can be taken directly from the linear Taylor Series expansion. DOT uses satisfaction of the Kuhn-Tucker Conditions to determine when it has reached a solution. Three additional considerations are checked to prevent unnecessary iterations. The routine will end if a maximum number of iterations (defined by the user) is exceeded or if conflicting constraints prevent a feasible solution within 20 iterations. The third condition is a user defined tolerance which sets a minimum required change in the objective function after each iteration. If this condition is not met, asymptotic convergence is indicated and the optimization is terminated. [Ref. 11:pp. E-3 - E-36]

## C. OPTIMIZATION METHODOLOGY

A specific, iterative methodology for the optimization process was selected to ensure consistency throughout the many optimization cycles. Figure 3.2 illustrates the selected

methodology. Each optimization began by defining the constraints, variables and objective function for the optimization and visually checking their assignment in the various code and data files. The affected files were then renamed according to run number and saved. This resulted in time savings and increased ease when trying to reproduce optimization results. The next step in the selected optimization process was to find a geometry which met the defined constraints, to act as an initial starting point for the optimization routine. Experience in how each variable effected the final geometry was used to generate these initial configurations. After running the optimization routine, the results were analyzed. This included checking to ensure that the waverider met all constraints, had an aesthetically pleasing geometry and delivered acceptable performance. If the optimization either failed or delivered unacceptable results, the variable or constraint responsible had to be determined and corrected and the process begun again.

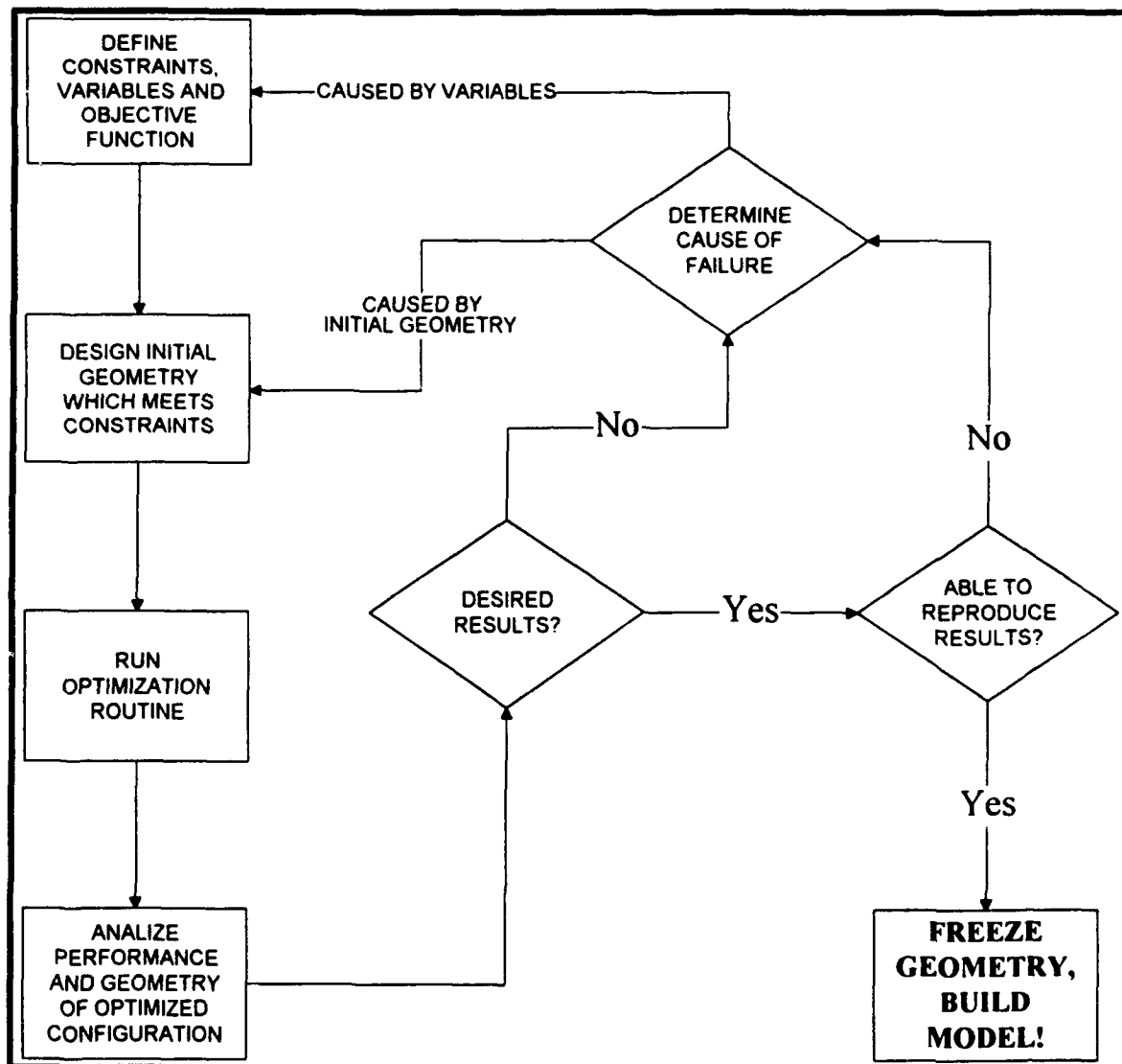


Figure 3.2 Optimization Flowchart.

## D. FIXED GEOMETRY PARAMETERS

Several parameters were selected to remain fixed during the optimization process. These parameters were derived from mission and performance requirements and included the vehicle length, combustor design, fairing start point and equivalence ratio.

### 1. Vehicle Length

Vehicle length is constrained by aircraft carrier operations. A sixty foot length was selected as the maximum total vehicle length based on current carrier-based aircraft. Table 3.3 lists lengths of various carrier-based aircraft upon which the length selection was made [Ref. 12].

**TABLE 3.3**  
**SIZE COMPARISON OF CARRIER-BASED AIRCRAFT**

AIRCRAFT	MISSION	SPAN	LENGTH
A-6 Intruder	all weather attack	53 ft 0 in	54 ft 9 in
F-14 Tomcat	fighter	64 ft 2 in	62 ft 8 in
E-2 Hawkeye	early warning/control	80 ft 7 in	57 ft 7 in
S-3 Viking	ASW	68 ft 8 in	53 ft 4 in
F-4 Phantom II	fighter/interceptor	38 ft 1 in	63 ft 0 in
F-18 Hornet	fighter/attack	37 ft 6 in	56 ft 0 in

### 2. Combustor

The SCRAMJET combustor (powerplant) uses a three inch throat height and five foot combustor length. Combustor width was allowed to vary during the optimization, as discussed later. Maximum combustor efficiency was assumed to be 0.95 for this design. Combustor efficiency is the fraction of injected fuel to burned fuel. Tables 3.4 and 3.5 list locations of expansions and injectors inside the combustor. Figure 3.3 shows combustor geometry. Internal locations in the combustor are given by station numbers which are multiples of throat height (i.e., station number 1 is located 3 inches from the throat).

**TABLE 3.4**  
**COMBUSTOR EXPANSION**

	Station	Distance from throat	Area Ratio ( $A_i/A_1$ )
$A_1$	0	0.0 in	1.0
$A_2$	4	12.0 in	1.1
$A_3$	20	60.0 in	3.0

**TABLE 3.5**  
**INJECTOR GEOMETRY**

Injector	Station	Distance from throat	Injector Angle	Injection Mach No.
1	3.75	11.25 in	30 deg	1.24
2	7.75	23.25 in	30 deg	2.07

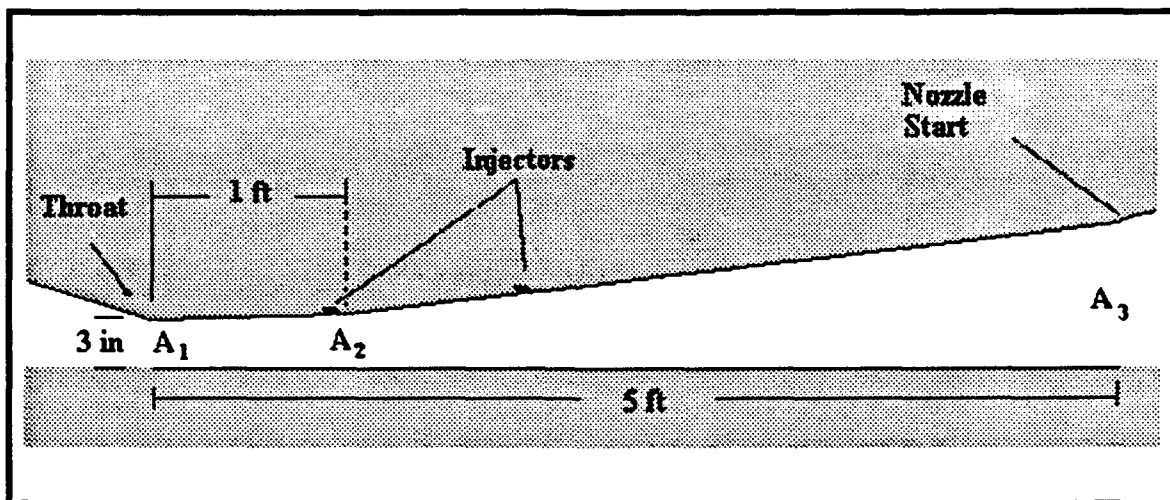


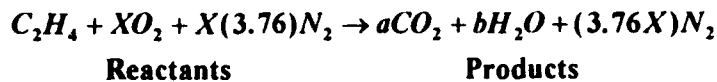
**Figure 3.3 Fixed Combustor Geometry.**

### 3. Equivalence Ratio

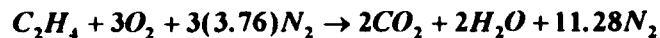
The equivalence ratio is a measurement of how close to stoichiometric a reaction is, as defined by the following equation:

$$\phi = \frac{\text{fuel / oxidizer}}{(\text{fuel / oxidizer})_{\text{Stoichiometric}}}$$

$\phi = 1$  indicates a stoichiometric reaction,  $\phi < 1$  indicates a fuel lean (air rich) mixture and  $\phi > 1$  indicates a fuel rich (air lean) mixture. A stoichiometric reaction is one where all of the oxygen atoms in the oxidizer react chemically to appear in the products. [Ref. 13:pp. 63-69] A simplified example of the reaction seen with the combustion of ethylene is given by:



For a balanced equation, X, a and b must be defined such that:



The air to fuel (AFR) ratio necessary to provide stoichiometric combustion is determined by the following equation:

$$AFR = \frac{N_{air}}{N_{fuel}} = \frac{(3 + 3.76(3))}{1} = 14.28 \text{ moles air / mole fuel}$$

On a weight basis:

$$AFR = 14.28(28.95) / 28 = 14.76 \text{ units air / unit fuel}$$

An equivalence ratio of 0.6 was used for the optimization of the hydrocarbon-powered waverider. This value was chosen, after experimenting with different values, as the one which prevented thermal choking in the combustor and also resulted in the

optimizer driving the combustor width to an acceptable value. Thermal choking is defined as the supersonic flow in the combustor being reduced to Mach 1 by heat addition [Ref. 14:pp. 77-85].

#### **4. Fairing Start Point**

The parabolic fairing designed by Pessin [Ref. 15] was added to the lower aft end of the waverider (see Figure 3.4). The fairing was used to reduce the base area, thereby reducing the base drag for increased transonic and low supersonic performance. In doing this, however, several penalties were suffered. Among these were a reduction in internal volume and a loss of L/D performance. There were two basic considerations in selecting the fairing start point. A fairing start located farther forward from the base resulted in a smaller initial angle for the fairing, decreasing the effects of flow separation. The forward point was limited, however, by the requirement of the fairing to be concave upward. If the fairing began too far forward the result was a convex fairing, resulting in increased drag. Additionally, the cruise L/D performance went down as the length of the fairing was increased. This made a tradeoff between initial fairing angle and fairing length necessary. Since the optimization routine does not consider the increased problem caused by base area at transonic and low supersonic speeds, it was not possible to use the fairing start point as an optimization variable. Thus, experimentation with different values using the Waverider Code was required to determine an acceptable fairing start point. This experimentation led to a choice of start location at 85% body length or 51 feet from the aircraft nose.

#### **5. Assumptions**

Overall vehicle density was assumed to be 25 lbs/ft<sup>3</sup>. A standard atmosphere was used for all calculations and the ratio of specific heats was assumed to be 1.4.



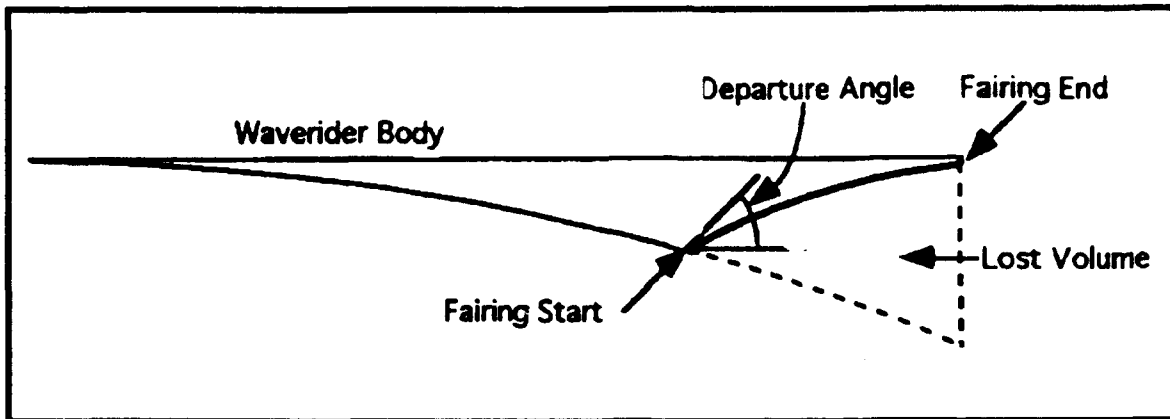


Figure 3.4 Pessin's Fairing Geometry. From Ref. 15.

## E. OPTIMIZATION CONSTRAINTS

Constraints were placed on the optimization of the waverider in order to meet projected mission and engine requirements and to produce an aesthetically pleasing body shape. Specific constraints used during the optimization included: internal body volume, span to length ratio, contraction ratio, maximum leading edge temperature, level unaccelerated cruise, and a requirement that the cowl shock hit the combustor inlet shoulder.

### 1. Volume

Required volume was based on the preliminary mission analysis and sizing studies as discussed in Section II. The actual constraint used was a volume factor of 1.5% of the body length cubed. For a 60 foot long waverider this gives a minimum volume of 3240 cubic feet. This results in an 81,000 pound aircraft at the assumed density of 25 lbs/ft<sup>3</sup>.

### 2. Span to Length Ratio

A maximum S/L of 1.0 was chosen primarily to give a balanced appearance. Additionally, this leads to a reasonable maximum wingspan at the trailing edge of 60 feet

for carrier based operations. Table 3.1 lists spans of various carrier-based aircraft for comparison.

### 3. Contraction Ratio

Contraction Ratio is a measure of external compression based on the size of the captured streamtube and throat height:

$$CR = \frac{\text{captured freestream area}}{\text{inlet area}}$$

Contraction Ratio was constrained to a minimum of 12.0 for this optimization.

Figure 3.5 shows the external compression shocks and contraction ratio geometry.

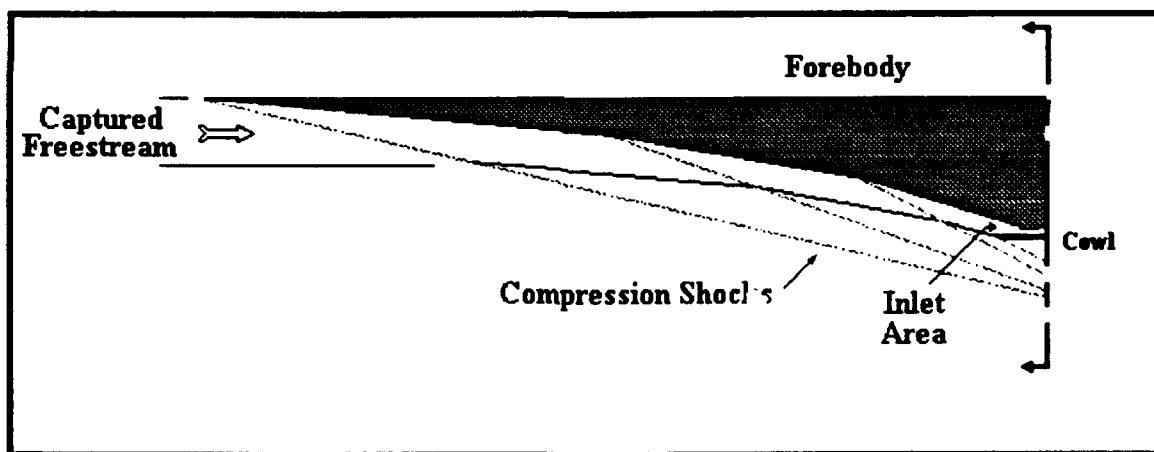


Figure 3.5 Contraction Ratio Geometry.

### 4. Unaccelerated Level Flight Requirements

To achieve unaccelerated, level flight during the cruise phase of the mission, the forces acting on the aircraft must be balanced. Normally these forces are lift, drag, thrust

and weight. For unaccelerated flight, thrust (T) must equal drag (D). Similarly, for level flight, lift (L) must equal weight (W). At the speed and altitude considered for this mission, however, another force becomes significant. It is the centrifugal force generated by flying a flight path which accounts for the curvature of the earth. This centrifugal force acts in concert with the lift force to balance the aircraft's weight, thereby reducing the amount of lift required for level flight. Weight At Altitude ( $W_{alt}$ ) is defined as the aircraft weight minus the centrifugal force. Lift was required to equal  $W_{alt}$  during cruise. These requirements are summarized below and depicted in Figure 3.6.

$$T = D$$

$$W_{alt} = W - F$$

$$L = W_{alt}$$

where: T=thrust

D=drag

W=weight

F=centrifugal force

L=lift

$W_{alt}$ =weight at altitude

## 5. Leading Edge Temperature

Maximum leading edge temperature was constrained to 3250 °R.

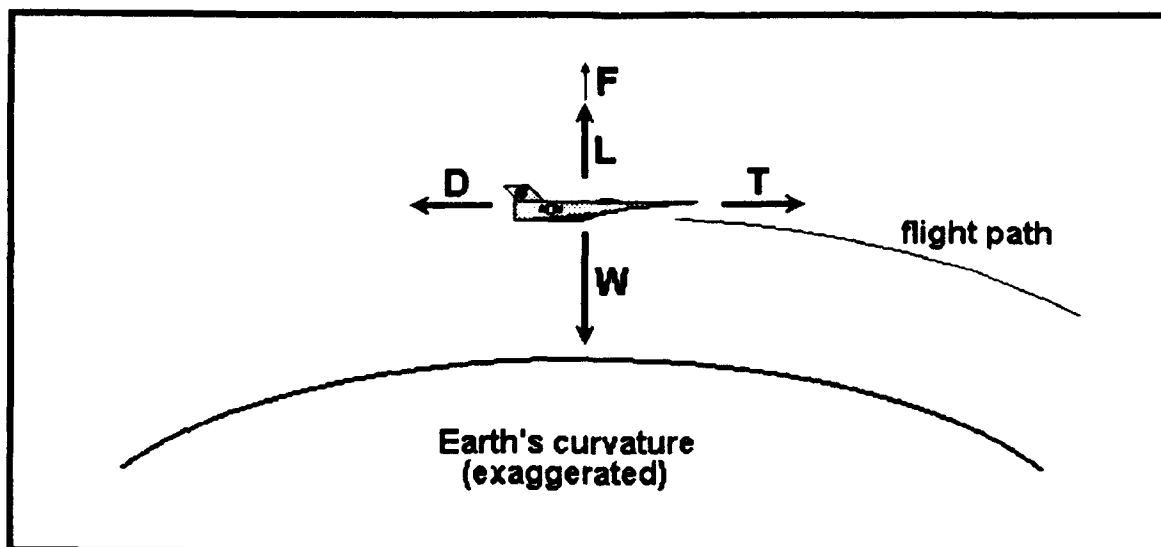


Figure 3.6 Forces Acting During Level Unaccelerated Cruise.

## 6. Shock on Shoulder

During an early optimization run of a hydrogen powered waverider, the optimization process was requiring the cowl to be too far forward in order to increase the objective function. This resulted in increased compression, thereby increasing engine performance, by using reflected shocks inside the cowl prior to the throat. On an actual aircraft boundary layer effects behind these reflected shocks would probably lead to engine unstart. In order to prevent this process, a constraint was introduced into the optimization routine which required the cowl shock to fall on the inlet shoulder. This constraint was met by calculating a "Shock on Ramp" ratio.  $X_r$  and  $X_s$  are the locations in percent body length of the cowl shock and ramp intercept and inlet shoulder, respectively. A tolerance of approximately 1 inch prior to the inlet shoulder was allowed in the optimization. For a body length of 60 feet, this leads to a Shock on Ramp ratio of 0.998. Figure 3.7 shows this "shock on ramp" geometry.

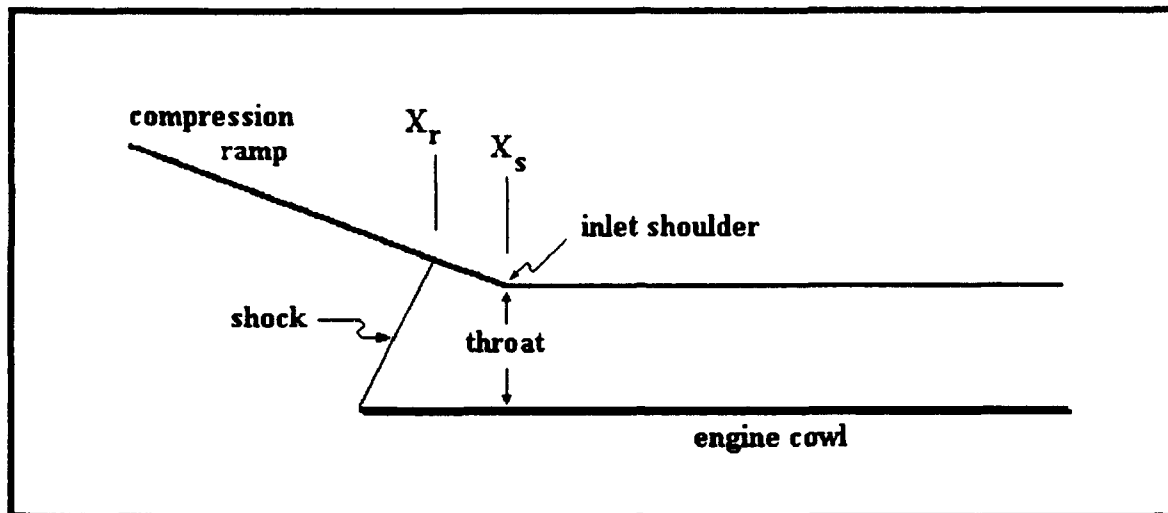


Figure 3.7 Shock on Ramp Geometry.

## F. OPTIMIZATION VARIABLES

Optimization variables included parameters which defined the waverider body and propulsion system geometry and the flowfield from which the waverider was derived.

### 1. Generating Curve

Input geometry variables include the first 6 coefficients which define the freestream trailing edge or generating curve (shown below).  $C_7$  and  $C_8$  were set to zero for this design. The generating curve is described by Figure 3.8. Table 3.6 lists coefficient limits for the optimization.

$$X = C_1 \tan \theta_s + C_2 Y + 10C_3 Y^2 + 100C_4 Y^3 + 1000C_5 Y^4 + 10,000C_6 Y^5 + C_7 \cos(1.570796C_8 Y / \tan \theta_s)$$

where:  $\theta_s$  = shock angle of the conical flowfield

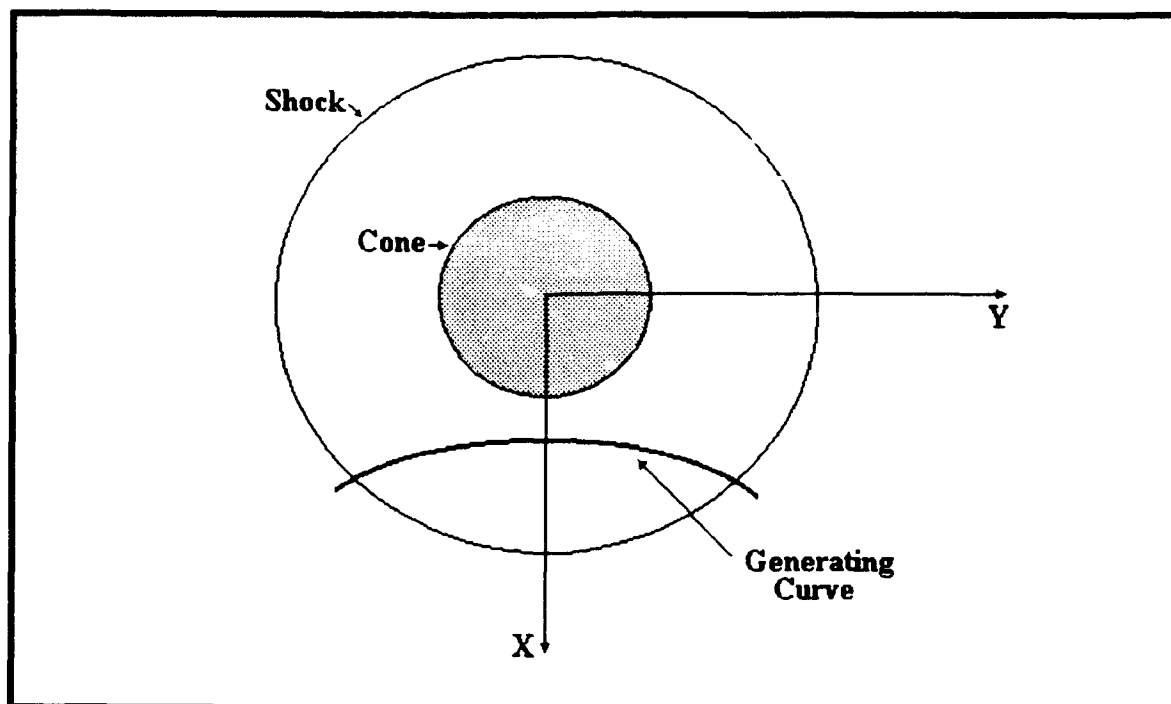


**Figure 3.8 Generating Curve Geometry (Aft View).**

**TABLE 3.6  
GENERATING CURVE COEFFICIENTS**

	lower limit	upper limit	initial value
C <sub>1</sub>	0.1	0.98	0.779
C <sub>2</sub>	0.0	0.95	0.047
C <sub>3</sub>	0.0	1.0	0.027
C <sub>4</sub>	-0.5	2.0	0.044
C <sub>5</sub>	-0.5	2.0	0.054
C <sub>6</sub>	0.0	2.0	0.014

## **2. Propulsion System Geometry**

A series of ramps on the underside of the aircraft is used to generate shocks which achieve the external compression of the air used by the scramjet. The geometry of these "compression ramps" is described by the angle and start locations of the ramps. Engine cowl geometry variables include the cowl start point and length. The initial nozzle angle

was also allowed to vary for the optimization. Table 3.7 lists the limits and initial values for these variables used during the optimization of the hydrocarbon configuration. Figure 3.9 depicts propulsion geometry.

**TABLE 3.7**  
**PROPULSION SYSTEM GEOMETRY VARIABLES**

	lower limit	upper limit	initial value
ramp 1 start	0.27	0.4	0.33
ramp 1 angle	2.0	5.0	4.9
ramp 2 start	0.42	0.55	0.53
ramp 2 angle	2.0	7.0	6.8
shoulder location	0.602	0.69	0.64
cowl leading edge	0.55	0.65	0.61
cowl length	0.25	0.33	0.3
nozzle start angle	20.0	40.0	25.0
angles in degrees			
locations in fraction of body length			

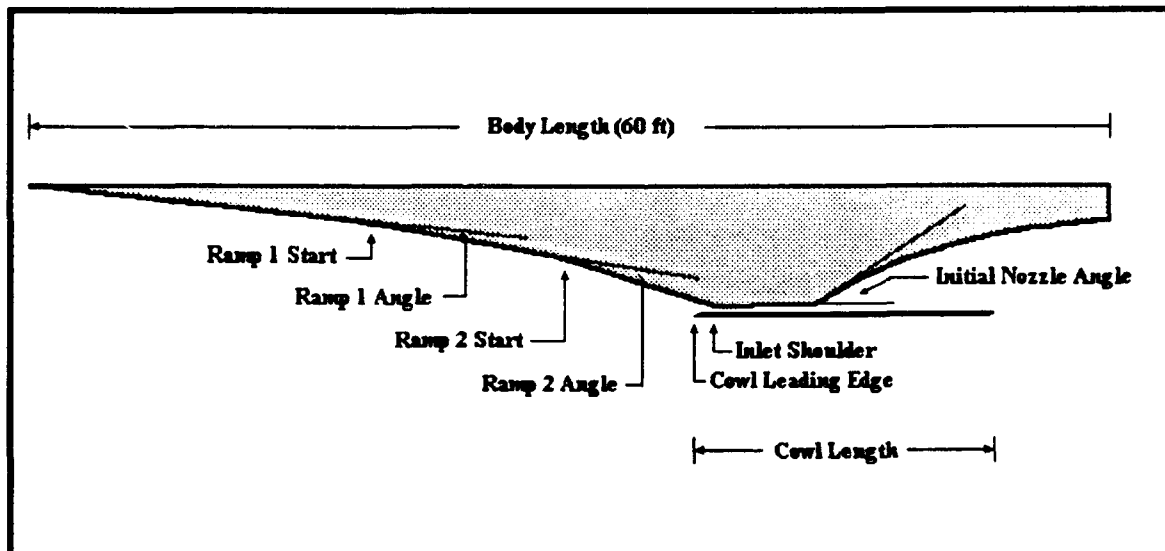


**Figure 3.9 Propulsion System Geometry.**

### **3. Leading Edge Radius**

The leading edge radius of the waverider was allowed to vary between .0625 and 1.0 inches. The initial value for optimization was set at 0.5 inches. A 0.5 inch leading edge radius was selected from previous waverider configurations as one which would result in a leading edge temperature of less than 3250 °R.

### **4. Generating Flowfield Shock Angle**

The shock angle of the conical flowfield from which the waverider was derived was also allowed to vary during the optimization. The best L/D performance of several of Bowcutt's viscous optimized Mach 6 conical-flow derived waveriders occurred at a shock angle of 12 degrees [Ref. 16:p. 11]. From this information it was decided to let the shock angle vary near this value. From experience with prior waveriders it was noted that shock angles above 13 degrees led to poor L/D performance when the span to length was constrained to 1.0 and shock angles below approximately 11 degrees resulted in unacceptably low internal volume. Hence, the upper and lower limits were set at 13 and 11 degrees, respectively. The initial value for the optimization calculations was 12.774 degrees.

### **5. Fairing Start Angle**

The initial angle for the parabolic fairing was allowed to vary between 10 and 45 degrees. The initial angle for optimization was set at 20 degrees.

## **G. OBJECTIVE FUNCTION**

As discussed previously, the product of L/D and specific impulse was used as the objective function for optimization. The logic behind maximizing this value comes from the Bréguet Range Equation (for jets) shown below. Since the Bréguet Range accounts for propulsive efficiency, heat content of the fuel and aerodynamic performance (L/D), it



can be considered a "figure-of-merit for the whole aircraft" [Ref. 1 pp. 6-7]. It can be seen from the equation that increases in either  $L/D$  or  $I_{sp}$  lead to proportional increases in range for a given velocity and fuel.

$$R = H \eta_p \frac{L}{D} \ln \frac{W_f}{W_i}$$

$$I_{sp} = \frac{H \eta_p}{V}$$

$$R = I_{sp} V \frac{L}{D} \ln \frac{W_f}{W_i}$$

where:  $R$  = range

$H$  = calorific value of the fuel

$\eta_p$  = propulsive efficiency

$W_f/W_i$  = segment weight fraction

$V$  = velocity

$I_{sp}$  = specific impulse

#### IV. OPTIMIZATION RESULTS

As discussed in Section III, the objective of this study was to optimize a hydrocarbon-powered waverider for the product of  $L/D$  and  $I_{sp}$ , while meeting several size and performance constraints. A solution for an optimum hydrocarbon-powered waverider was found by the optimization routine which met all of the constraint functions. At the optimum solution, two of the seven constraint functions, Shock on Ramp and Contraction Ratio, were active. An active constraint is one in which the optimization routine is forced to "march" along the constraint function in order to increase the objective function and satisfy the constraint, rather than moving in the direction of the gradient. Fewer active constraints increases the likelihood of solving for the true maximum of the objective function in the local space being considered. The resulting flow properties, body geometry and propulsion system geometry of this optimum solution for a hydrocarbon-powered configuration are discussed below.

##### A. FLOW PROPERTIES

Table 4.1 contains free stream flow properties and flow properties at the cowl lip and combustor inlet for the optimum configuration's calculated cruise altitude of 85,226 ft.

**TABLE 4.1**  
**OPTIMUM CONFIGURATION FLOWFIELD SUMMARY**

	MACH	PRESS (psf)	TEMP (R)	VEL (ft/s)	RHO (lb/ft <sup>3</sup> )
Free Stream	6.00	0.3188	400.520	5886.2	0.000067
Cowl Lip	4.156	2.388	739.238	5528.753	1.841
Combustor Inlet	2.493	17.9	1474.563	4612.627	0.001018

## B. OPTIMUM BODY GEOMETRY

Specific results from the optimized hydrocarbon-powered waverider body geometry are discussed individually below and are summarized in Table 4.3. As discussed in Section III, shock angle and generating curve coefficients were varied during the optimization process. The values of these variables which led to the optimum configuration and the resulting body geometry are summarized below. Figure 4.1 depicts the resulting optimum configuration.

### 1. Generating Shock Angle

The angle of the conic shock which defines the flowfield from which the resulting optimum hydrocarbon-powered waverider is derived was selected as 12.9892 degrees by the optimization routine.

### 2. Generating Curve

The coefficients of the generating curve which defines the upper surface of the optimized hydrocarbon-powered waverider chosen by the optimization routine are listed in Table 4.2. It is noteworthy that all of the coefficients are positive. This leads to a simple curvature of the upper surface and would likely result in less expensive manufacturing costs for an actual aircraft.

**TABLE 4.2**  
**GENERATING CURVE COEFFICIENTS FOR OPTIMUM CONFIGURATION**

C <sub>1</sub>	C <sub>2</sub>	C <sub>3</sub>	C <sub>4</sub>	C <sub>5</sub>	C <sub>6</sub>
0.760425	0.049392	0.029621	0.047527	0.57519	0.014328

### 3. Span

The S/L of the optimized configuration is 0.9419. This was a direct result of the tradeoff between the contraction ratio constraint and trying to maximize  $L/D \cdot I_{sp}$ . Trends from the initial non-optimized waveriders indicated that, in general,  $L/D$  increased with

increased S/L. In order to achieve this increase in S/L, however, the waverider is generated lower (farther from the cone axis) in the conical flowfield. This leads to smaller contraction ratios and reduced engine performance. The resulting planform has a span of 56.51 ft and a plan area of 2266.33 ft<sup>2</sup>. From this, Aspect Ratio is calculated below to be 1.41 [Ref. 17:p. 158].

$$AR = \frac{b^2}{S} = \frac{(56.51)^2}{2266.33} = 1.41$$

where: b = wing span

S = plan area

#### **4. Internal Volume**

Internal volume is important because it determines the amount of fuel capable of being carried and, in turn, the aircraft's range. Volume Factor for the optimized configuration is 2.075 percent of the body length cubed. This leads to a volume of 4481.04 ft<sup>3</sup> and a weight of 112,025.93 lbs.

#### **5. Leading Edge Radius**

The leading edge radius of the optimized configuration is 0.4995 inches. This value is a result of the tradeoff during the optimization between leading edge temperature and drag. As the leading edge radius goes up, drag increases and temperature decreases. Similarly, as the leading edge gets sharper, the temperature increases and the drag decreases. It is desirable for a waverider to have as sharp an edge as possible in order to keep the shock attached to the leading edges.

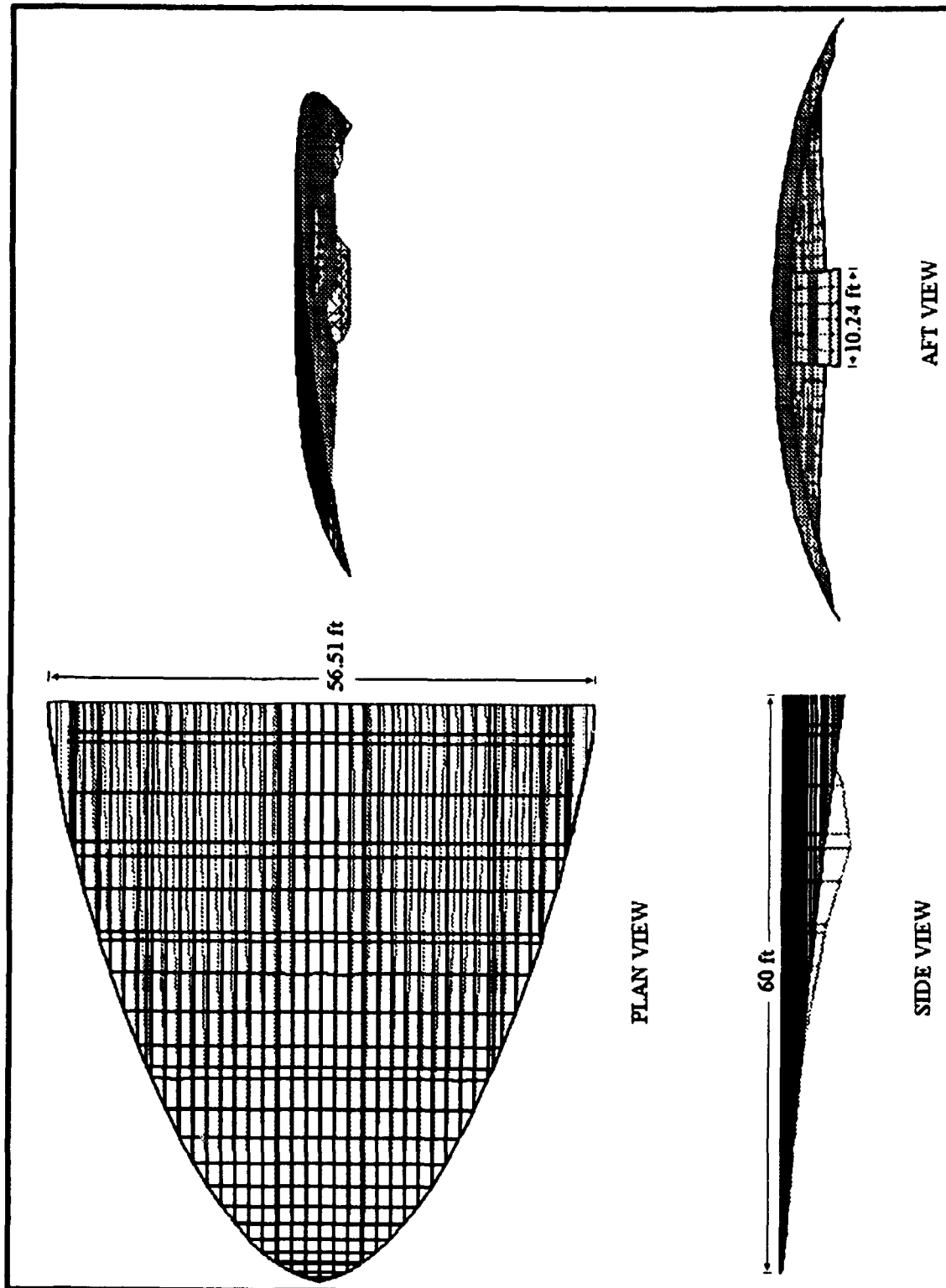


Figure 4.1 Resulting Optimum Configuration.

**TABLE 4.3**  
**OPTIMIZED CONFIGURATION BODY GEOMETRY**

Length	Span	Plan Area	AR	Volume	Weight	Lead Edge Radius
60 ft	56.51 ft	2266.33 ft <sup>2</sup>	1.41	4481.04 ft <sup>3</sup>	112,025.9 lbs	0.4995 in

### C. OPTIMUM PROPULSION SYSTEM GEOMETRY

The engine geometry parameters of the optimized hydrocarbon-powered configuration are summarized in Table 4.4. Combustor width of the optimum configuration is 10.238 ft. The forebody ramps, cowl and nozzle all share this width. The optimum configuration's propulsion system geometry is depicted in Figure 4.2.

**TABLE 4.4**  
**OPTIMIZED CONFIGURATION PROPULSION SYSTEM GEOMETRY**

	Start Location	Start Angle (deg)	Length
Nose	0.0	5.1293	19.923
Ramp 1	0.33205	4.99871	11.941
Ramp 2	0.53107	6.99774	7.704
Combustor	0.65947		5.0
Cowl	.63175		17.999
Nozzle	.74280	24.99959	15.432

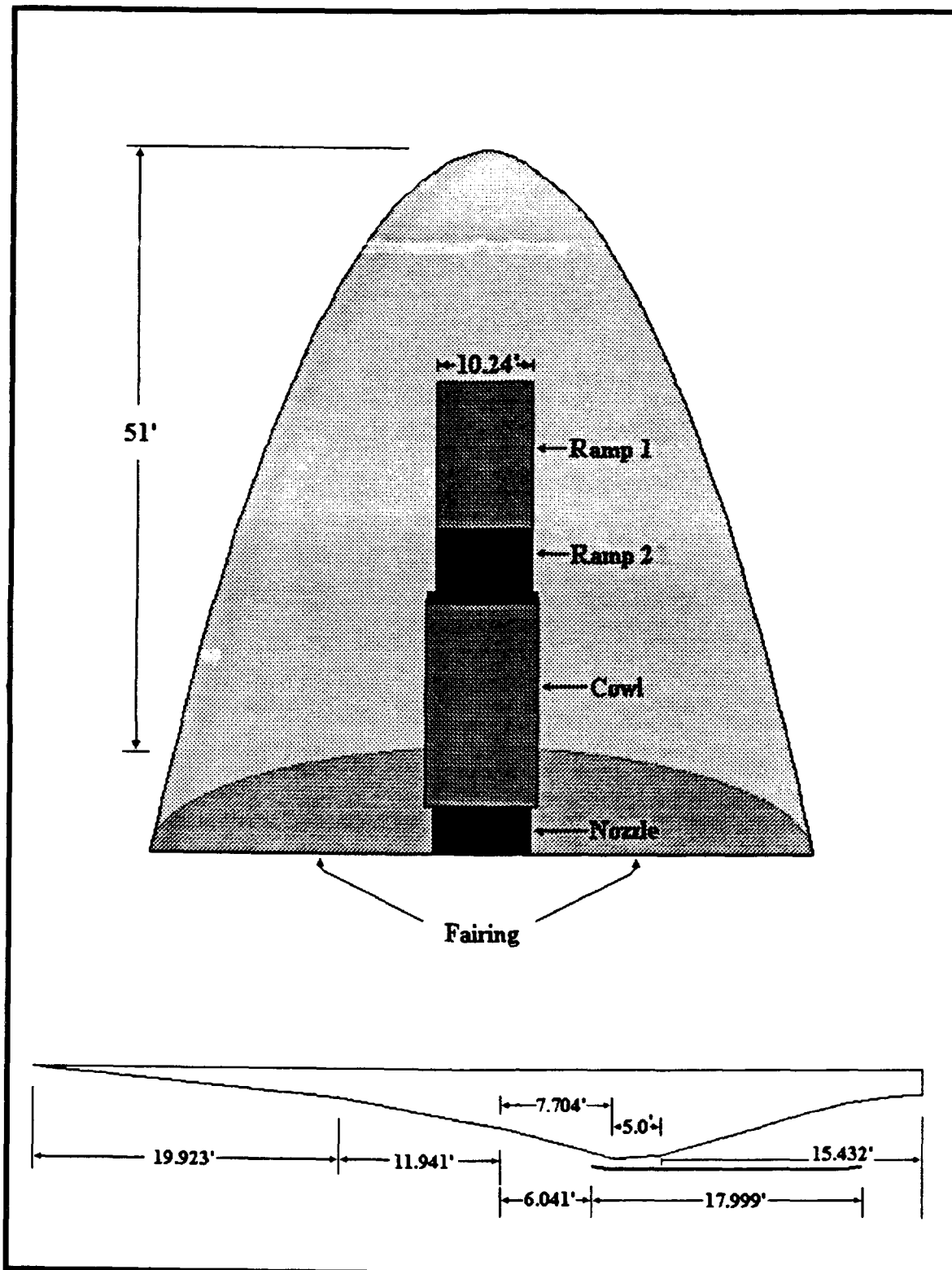


**Figure 4.2 Optimized Configuration Propulsion System Geometry**

#### D. OPTIMUM CONFIGURATION PERFORMANCE

As discussed in the previous chapter, several constraints and an objective function were placed on the optimization process. All constraints were met by the resulting optimum hydrocarbon-powered configuration. Contraction Ratio and Shock on Shoulder Ratio were active at the optimum solution. Table 4.5 summarizes the optimized configuration's cruise performance as computed by the Waverider Code.

**TABLE 4.5**  
**OPTIMIZED CONFIGURATION PERFORMANCE SUMMARY**

CONSTRAINT	LIMIT	VALUE FOR OPTIMUM
Contraction Ratio	$\geq 12.0$	11.940
Lift	= Weight at Altitude ( $W_{alt}$ )	Lift = 106544.23 lbs $W_{alt}$ = 106258.07 lbs
Thrust	= Drag	Thrust = 27211.00 lbs Drag = 27039.75 lbs
Shock on Shoulder Ratio	$\geq 0.998, \leq 1.0$	0.996
Volume Factor	$\geq 0.015$	0.021
Leading Edge Temp.	$\leq 3250$ R	2589.5 R
Span to Length Ratio	$\leq 1.0$	0.9419
Cruise L/D		4.176

#### E. COMPARISON WITH PRELIMINARY SIZING RESULTS

Table 4.6 compares the optimized configuration with initial sizing results. The optimum configuration weight is for cruise. The preliminary sizing weights are at takeoff.

**TABLE 4.6**  
**COMPARISON WITH PRELIMINARY SIZING**

	PRELIMINARY SIZING	OPTIMUM CONFIG.
WEIGHT	100,000 ( max carrier) 120,600 (first order )	112,026
LENGTH	60 ft	60 ft
SPAN	60 ft	56 ft 6 in
PLAN AREA	2670 ft <sup>2</sup>	2266 ft <sup>2</sup>
ASPECT RATIO	1.35	1.41
WING LOADING	45 lbs/ft <sup>2</sup>	50 lbs/ft <sup>2</sup>



## V. PERFORMANCE PREDICTION AND COMPARISONS

Aerodynamic performance predictions were made using the VORLAX and Waverider codes at NASA Ames Research Center. The VORLAX code is a vortex lattice code that uses Polhamus' Leading Edge Suction Analogy. Briefly, Polhamus' theory accounts for flow reattachment inboard of the leading edge when calculating total lift [Ref. 8:p. 20]. This flow reattachment is caused by the normal force imparted by the vortex flow reenergizing the upper surface boundary layer.

Lowspeed performance predictions (specifically  $C_L$ ) are used in Section VI as a basis for wind tunnel model sizing and to predict forces measured in the tunnel. A comparison is made between predicted performance of the optimized hydrocarbon-powered configuration of this study, Vanhoy's lowspeed tested Mach 6 waverider [Ref. 8], one of Bowcutt and Anderson's Mach 6 viscous optimized waveriders [Ref. 16] and historical trends.

### A. COEFFICIENT OF LIFT

The coefficient of lift,  $C_L$ , is needed to predict forces seen in the wind tunnel. The first method used in predicting  $C_L$  was low aspect ratio wing theory as given by the equation below. The resulting value multiplied by  $\alpha$  (in radians) results in values for  $C_L$  versus  $\alpha$ .

$$C_{L_{\infty}} = \frac{\pi}{2} AR = \frac{\pi}{2}(1.41) = 2.215$$

Additionally, as noted by Pope [Ref. 18:p. 287], the  $C_L$  curve for aspect ratios below three can be approximated by:

$$\frac{dC_L}{d\alpha} = 0.008 + 0.018AR \text{ (per degree)}$$

Finally, a vortex lattice analysis was performed on the optimized hydrocarbon-powered configuration of this study by the Systems Analysis Branch, NASA Ames Research Center using the VORLAX code. One result of the VORLAX code is a prediction of  $C_L$  at differing angles of attack and Mach numbers.  $C_L$  values were predicted by the VORLAX run for Mach numbers of 0.2 and 0.235 in anticipation of planned lowspeed wind tunnel tests. Angle of attack for these computations was varied from 0 to 20 degrees.

The resulting  $C_L$  versus  $\alpha$  values for both Low Aspect Ratio Theory and the VORLAX code are listed in Table 5.1. These results are also plotted in Figure 5.1. From the figure it can be seen that the slopes of the curves are almost identical. The values from the VORLAX code are slightly lower than those from Low Aspect Ratio Wing Theory. This is most likely a result of the slightly negative mean camber distribution of the waverider body as computed by the VORLAX code.

**TABLE 5.1**  
 **$C_L$  VALUES FROM LOW AR THEORY AND VORLAX**

AOA	Low AR Theory	Pope	VORLAX	
			Mach 0.2	Mach 0.235
0	0	0.008	-0.07546	-0.07582
2.5	0.09663	0.07145	0.00421	0.00398
5.0	0.1933	0.1349	0.08414	0.08405
7.5	0.2899	0.19835	0.16411	0.16417
10.0	0.3865	0.2618	0.24276	0.24295
15.0	0.5798	0.3887	0.39534	0.39580
20.0	0.7731	0.5156	0.53918	0.53987

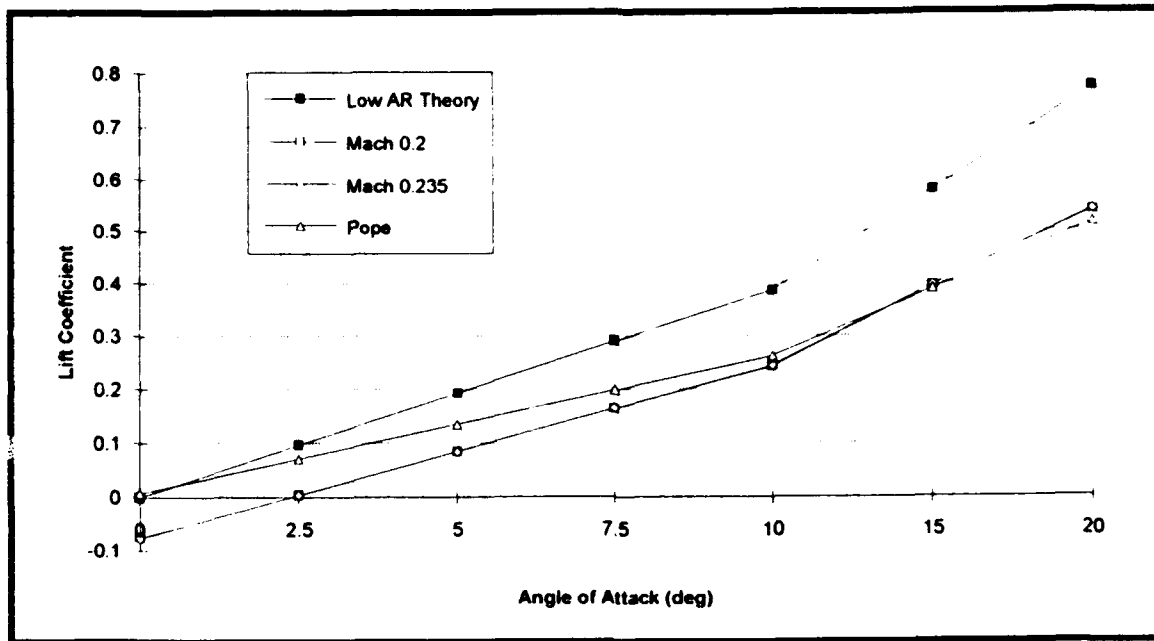


Figure 5.1  $C_L$  vs  $\alpha$ .

## B. CRUISE PERFORMANCE

Increased cruise performance makes waveriders generally better suited to hypersonic flight than other configurations. Of course, this advantage in cruise performance is based on the condition that the waverider be operating "on design"; the Mach number it is designed for and at zero angle of attack. When on design, waveriders have shown impressive results. Figure 5.2 shows a L/D comparison between three hypersonic configurations [Ref. 18:p. 28].

L/D at cruise for the optimum hydrocarbon powered configuration of this study is substantially lower than Bowcutt and Anderson's Mach 6 viscous optimized waveriders. As shown by Figure 5.3, the L/D of their best optimum Mach 6 waverider ( $\theta_s=12^\circ$ ) is over 8.0 [Ref. 16:p. 28]. The lower L/D performance (4.17) of the waverider configuration of this study is directly attributed to the addition of the fairing and propulsion system. Table 5.2 summarizes this comparison.  $C_L$  for the configuration of

this study was computed at Mach six and zero angle of attack using the VORLAX code.

The volumetric efficiency is given by:

$$\eta = \frac{V^{2/3}}{S_p} = \frac{4481.04^{2/3}}{2266.33} = 0.12$$

where: V = internal volume

S<sub>p</sub> = plan area

**TABLE 5.2**  
**CRUISE PERFORMANCE COMPARISON**

	Bowcutt's Optimum	Powered Optimum
Volumetric Efficiency, $\eta$	0.12	0.12
C <sub>L</sub>	0.045	0.0084
L/D	8.1	4.2

### C. LOW SPEED PERFORMANCE COMPARISONS

Comparisons of low speed results by Vanhoy [Ref. 8] indicated good agreement between Polhamus' Theory, a Mach 6 viscous optimized waverider, and a delta wing of similar length and span as shown in Figure 5.4 [Ref. 8:p. 41]. Similar performance should be expected by the configuration generated by this study. For comparison, the C<sub>L</sub> values computed by the VORLAX code have been overlaid on Figure 5.4.

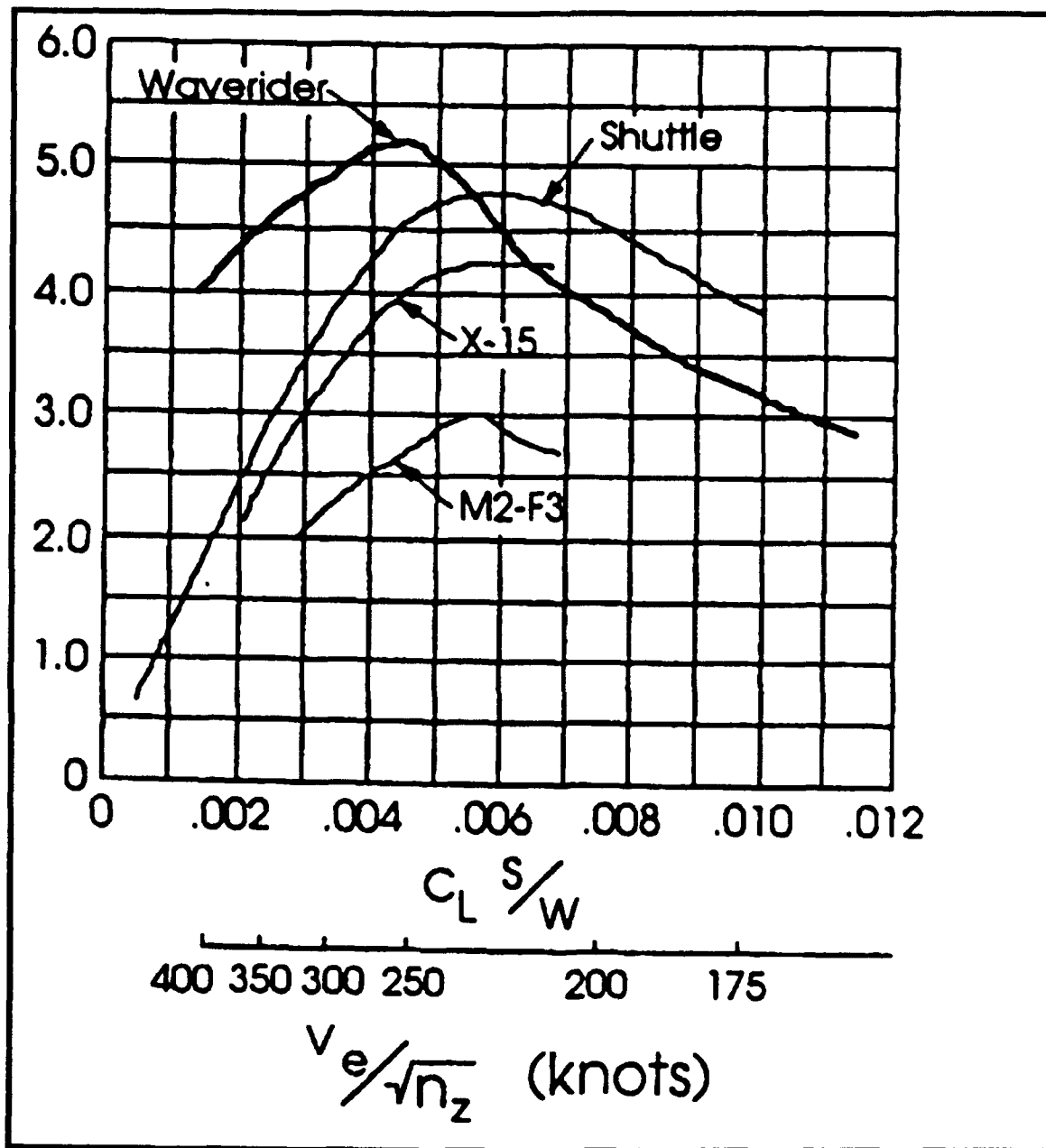


Figure 5.2 Hypersonic Configuration Performance Comparison. From Ref. 19.

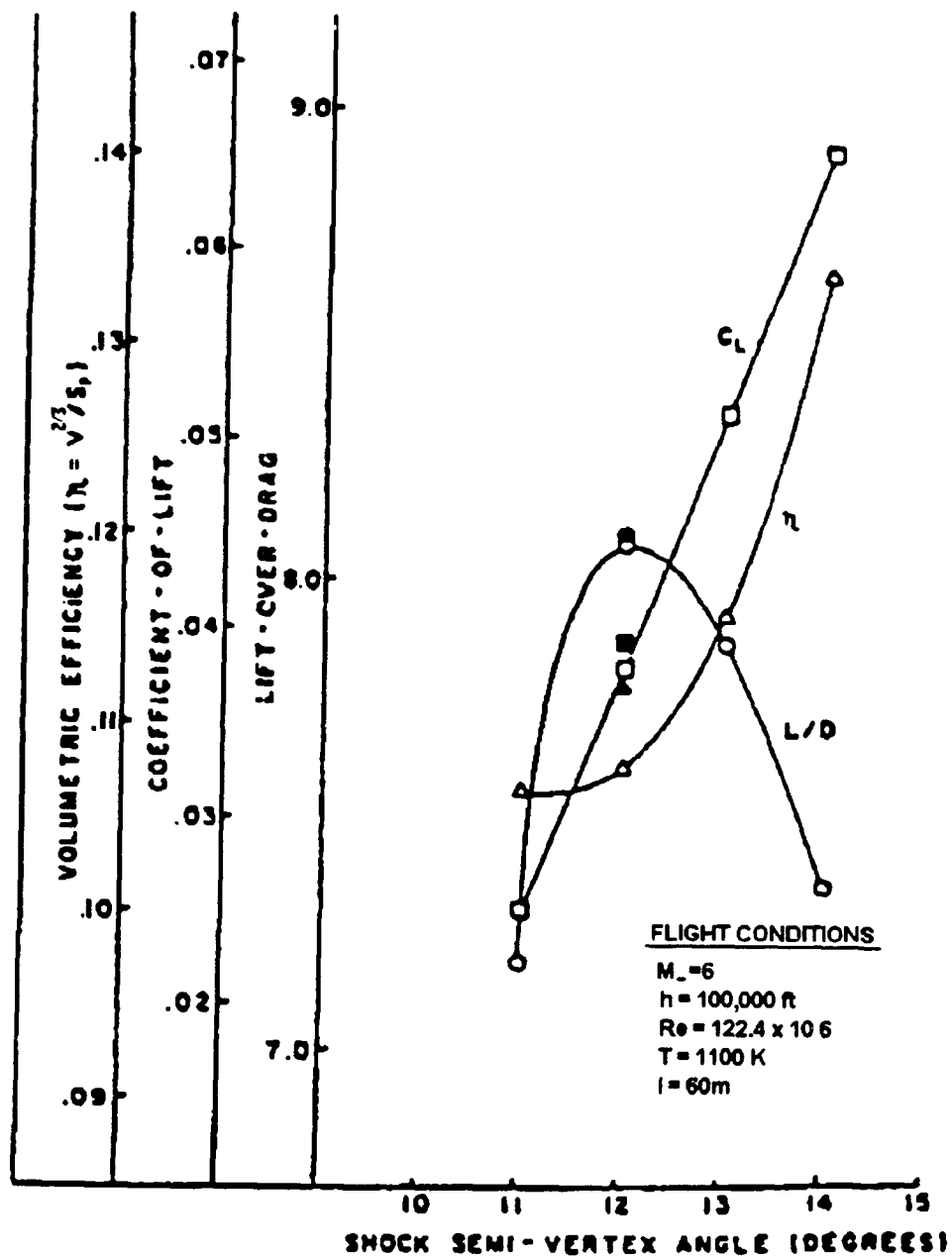


Figure 5.3 Results for a Series of Optimized Mach 6 Waveriders From the University of Maryland. From Ref. 16.

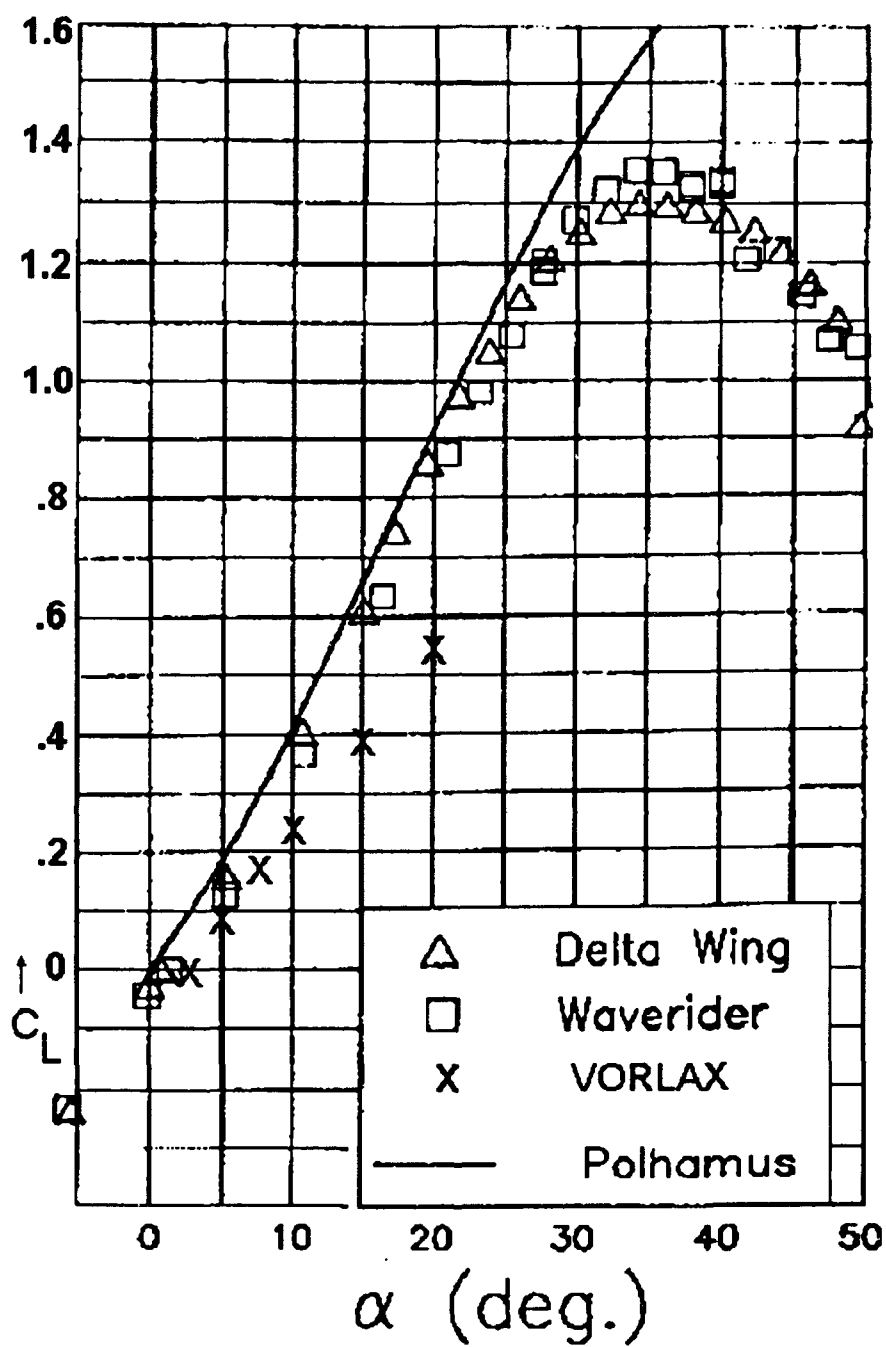


Figure 5.4  $C_L$  Comparisons. From Ref. 8.

## **VI. TEST PREPARATION**

Low speed testing is important in determining the viability of any aircraft. It is critical for carrier based aircraft due to their low takeoff and approach speeds. Wind and water tunnel tests are planned for Summer 1993.

### **A. WIND TUNNEL TESTS**

Low speed wind tunnel tests will be conducted using a 15 inch long aluminum model in the 32 inch by 45 inch wind tunnel at the Naval Postgraduate School. Low speed testing is intended to investigate the speed regime below approximately 150 knots; typical of carrier-based aircraft approach speeds.

#### **1. Wind Tunnel Description**

The wind tunnel planned for use is a closed circuit, single return, horizontal flow wind tunnel. Power is provided by a 100 horsepower electrical motor coupled to a three-bladed variable pitch fan via a four-speed truck transmission. The tunnel has a contraction ratio of 10:1 and a test section length of 48 inches. The maximum test section velocity is 260 ft/sec with a nominal freestream turbulence level of 0.2%. Hinged glass windows on both sides and a window in the ceiling provide easy access and viewing. [Ref. 20:pp. 598-599] Figure 6.1 shows the planned installation of the waverider in the wind tunnel.



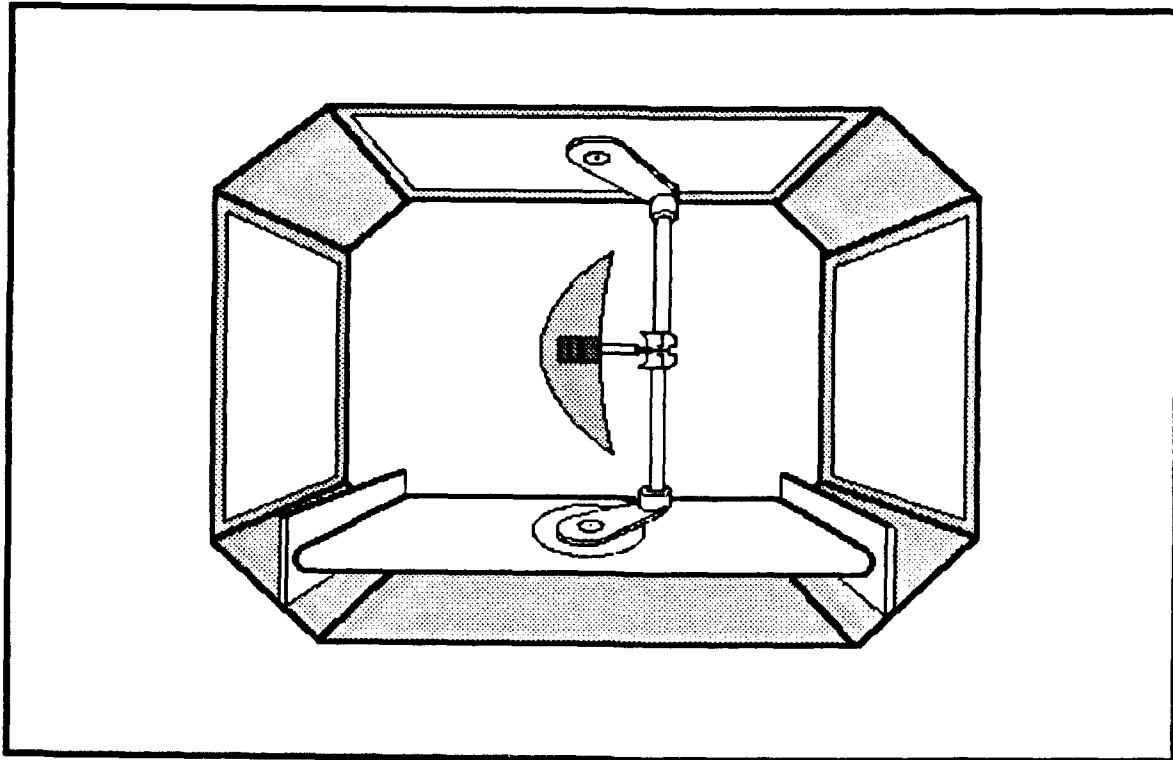


**Figure 6.1 Planned Installation of Optimized Hydrocarbon-Powered Waverider in NPS 32x45 inch Wind Tunnel. After Ref. 20.**

## **2. Test Parameters**

Initial low speed testing will gather force and moment data from -10 to +20 degrees angle of attack. A sting mounted, six component internal strain gage balance will be used to measure the forces and moments experienced by the model in the wind tunnel. These measurements will yield lift, drag and side forces and pitching, rolling and yawing moments [Ref. 18:p. 126].

## **B. WATER TUNNEL TESTS**

Flow visualization tests will be performed in the Naval Postgraduate School Flow Visualization Water Tunnel Facility. This is a horizontal, continuous flow tunnel with a 15

inch wide, 20 inch high and 60 inch long test section. Glass construction allows easy viewing of the model during tests. Maximum water velocity in the test section is approximately one foot per second with a nominal RMS freestream turbulence level of less than one percent. Flow visualization is affected by dye injection at points of interest on the model. Six pressurized lines route the dyes from the dye reservoir to the model. [Ref. 21:pp 1-2]

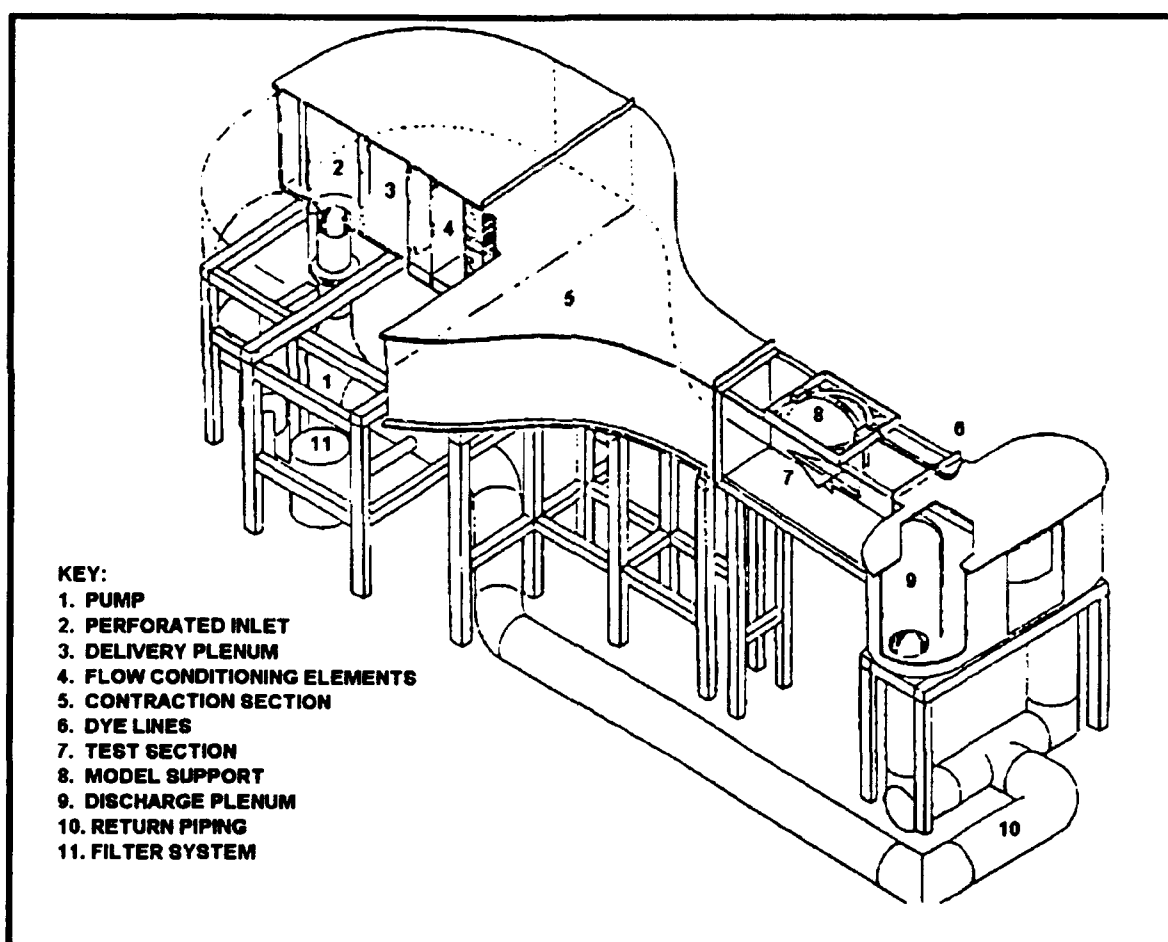


**Figure 6.2 The NPS Flow Visualization Water Tunnel Facility. From Ref. 21.**

## **C. MODEL PREPARATION**

Model preparation included material selection, balance selection and model sizing for both the wind and water tunnel models.

### **1. Wind Tunnel Model sizing**

Factors in choosing the model size included balance availability, wind tunnel test section size, and cost. The test section size of 32 by 45 inches limits the span of the model to approximately 18 inches. Appendix C contains model sizing calculations.

### **2. Balance Selection**

A listing of available sting mounted, internal strain gage balances was obtained from the balance shop at NASA Ames Research Center. Several balance diameters were available. Due to the small model size required by the NPS wind tunnel, the 0.75 inch diameter balance was selected. An iterative process led to the selection of a 15 inch model length and a balance with a total normal force capacity of 50 pounds. At 20 degrees angle of attack, the model is predicted to generate a normal force of approximately 40 pounds (see Appendix C).

### **3. Water Tunnel Model Sizing**

The major consideration in sizing the model for the flow visualization testing was flow blockage in the water tunnel test section. A limit of 5% flow blockage was used in sizing the water tunnel model. An 8 inch long model remains below this limit up to about 22 degrees angle of attack (see Appendix C).

### **4. Model Material and Construction**

Options considered for construction of the models included the computerized milling of aluminum, polyboard, or laminated mahogany models or the casting of epoxy resin models. Mahogany was ruled out for both wind and water tunnel tests due to its inability to hold the sharp leading edges required by the models. The radius of the leading

edges on the wind tunnel model will be approximately 1 mil. Additionally, it would be difficult to seal the mahogany model for water tunnel testing. Polyboard was ruled out due to its lack of stiffness. Epoxy resin suits itself to making many copies of the same model since it is formed from a mold. The expense of using it to make just one model, however, was prohibitive. Aluminum was chosen for both models because of its rigidity, its ability to hold an edge and its relatively low cost. The specific alloy chosen was 7075 aluminum, as recommended by the Ames machine shop. Table 6.1 contains material properties of 7075 aluminum alloy [Ref. 22:p. 245].

**TABLE 6.1**  
**7075 ALUMINUM PROPERTIES**

Property	Density	Ultimate Tensile Strength	Tensile Yield Strength	Young's Modulus	Shear Modulus
Units	$\text{kg/m}^3 \times 10^3$	$\text{N/m}^2 \times 10^6$	$\text{N/m}^2 \times 10^6$	$\text{N/m}^2 \times 10^9$	$\text{N/m}^2 \times 10^9$
Value	2.80	523	448	71	26.9

## **VII. FOLLOW-ON RESEARCH**

The design of any new aircraft creates research opportunities in every engineering field. This is especially true if the aircraft being designed is on the frontier of technology. Hypersonic waveriders fit this description and work is required in every field to determine if they are viable candidates for the high speed aircraft of the future. Material and structural analysis, control system design, thermal control, and application studies are just a few of the areas that come to mind. For the waverider configuration of this study, the existence of a set of models makes intensive, hands on aerodynamic analysis possible in the near term. This should add dramatically to existing waverider data bases.

### **A. PLANNED NEAR-TERM TESTING**

The next step in this joint, on-going study between the Naval Postgraduate School and the NASA Ames Research Center is the planned lowspeed wind tunnel and water tunnel tests for which the 15 inch and 8 inch models are currently being constructed. These tests are intended to gather force and moment data and flow visualization data, respectively. The results of both of these tests will undoubtedly lead to more opportunities for research.

The initial water tunnel tests will likely show whether or not the position of the vortex flows around the leading edges of the waverider are stable. If they are not, testing to determine if they can be made stable can be studied.

At 15 inches in length, the wind tunnel model is large enough to make the drilling of pressure taps at a later date relatively inexpensive. The material it is constructed of also makes testing in the higher subsonic and supersonic speed regimes possible.

## **B. ADDITIONAL AREAS FOR RESEARCH**

Several specific questions arose during this study that apply directly to the waverider configuration designed herein. Each could be complete projects in themselves. Among these, modifications to the Waverider Code to append tails and/or a cockpit to the waverider is a possibility. Heat transfer, emissions, structural requirements, internal packing studies and refined mission performance predictions should be studied. Additionally, optimization of waverider configurations for other specific missions including single-stage-to-orbit, aero-assisted orbital transfer vehicles, missiles and various aircraft missions can be studied. Research in each of these areas, and many not listed, will serve to move waveriders closer to actual vehicles. Figure 7.1 depicts a conceptual aircraft based on the waverider configuration generated by this study.

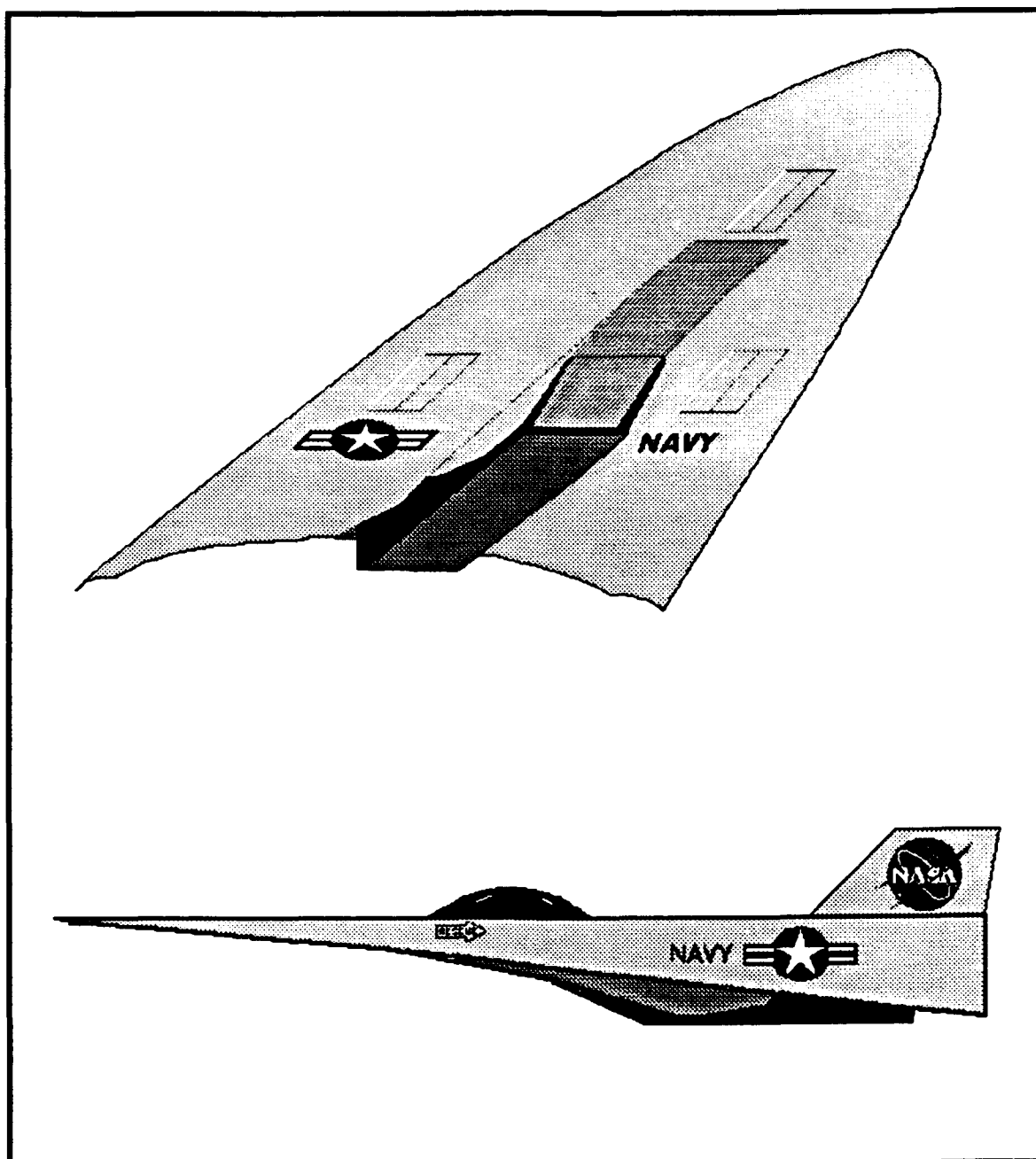


**Figure 7.1 Hydrocarbon-Powered Waverider Aircraft Configuration.**

## VIII. CONCLUSION

Arguably, the most valuable result of this research project has been the successful use of the Ames Waverider Code to generate a completely integrated engine/body waverider configuration optimized for a specific mission. The success of the Waverider Code in producing a viable powered waverider, with so many constraints placed on size, performance and appearance, attests to the code's robust nature and the programming talent of those who wrote it.

It is concluded that an integrated engine/body aircraft configuration, capable of meeting specific mission requirements (a deck-launched interceptor in this case), can be derived from a conical-flow waverider. As expected, the aerodynamic performance of such a configuration, when compared with an optimum pure waverider, is substantially lowered by the addition of a propulsion system and fairing. Additional penalties will certainly be suffered with the addition of a cockpit, fin and control surfaces.

This project has studied several considerations required to design, model and test an actual powered aircraft configuration based on a waverider. It is, however, only a first look at these requirements. It is recommended that studies in the optimization of waveriders for application to other real-world missions be undertaken. These studies should be of integrated engine/body designs with a view towards optimizing a specific desired mission performance. Only this type of research will answer whether or not waverider configurations can be viable vehicles.



## **APPENDIX A - PRELIMINARY AIRCRAFT SIZING**

A preliminary sizing study was done following Nicolai [Ref. 9] and Raymer [Ref. 10]. Preliminary sizing was based on historical trends and current data bases and was used for comparison with the optimized hydrocarbon configuration of this study. The basic result of preliminary sizing is to estimate gross takeoff weight and fuel weight required for the mission.

### **A. WING GEOMETRY**

Wing geometry is predicted for the given mission based on historical trends.

#### **1. Aspect Ratio**

One would expect that a delta-type planform waverider would have a low aspect ratio. Based on historical trends for jet fighters (non-dogfighters), the aspect ratio is estimated at 1.35 [Ref. 10:p. 53].

#### **2. Wing Area**

Based on the predicted aspect ratio and assuming the span is equal to 60 feet ( $S/L_{\max}=1.0$ ), the wing area,  $S$ , is equal to 2670 square feet.

$$S = \frac{b^2}{AR} = \frac{60^2}{1.35} = 2670 \text{ ft}^2$$

### **B. THRUST-TO-WEIGHT RATIO**

#### **1. Takeoff**

A statistical estimation of T/W for a jet fighter (non-dogfighter) gives a typical required installed T/W of 0.6 [Ref. 10:p.79]. Using two J-58 turbojets, each with 30,000

pounds of thrust at sea level [Ref. 9:p. 14-6], fills this requirement for a 100,000 pound aircraft.

## 2. Cruise

During level, unaccelerated cruise, the T/W must equal the inverse of L/D [Ref. 10:p. 81]. Cruise L/D was assumed to be 4.0 for this calculation.

$$[T/W]_{cruise} = \frac{1}{[L/D]_{cruise}} = 0.25$$

## C. TAKEOFF WEIGHT ESTIMATION

Takeoff weight is estimated using an iterative process based on an initial guess of takeoff weight, crew and payload weight, and calculated fuel and empty weight fractions as given below [Ref. 10:p. 12]. Fuel fraction assumes a 6% allowance for reserve and trapped fuel. [Ref. 10:p. 23]

$$W_0 = \frac{W_{crew} + W_{payload}}{1 - (W_f / W_0) - (W_e / W_0)}$$

$$\frac{W_f}{W_0} = 1.06(1 - \frac{W_x}{W_0})$$

where:  $W_0$  = takeoff weight

$W_{crew}$  = crew weight

$W_{payload}$  = payload weight

$W_f$  = fuel weight

$W_e$  = empty weight

$W_x$  = mission segment fuel fractions as calculated below

## 1. Initial Takeoff Weight Estimate

The initial weight guess for this aircraft was chosen to be 100,000 pounds based on the maximum takeoff gross weight for existing catapults from Figure A.1 [Ref. 10:p. 90].

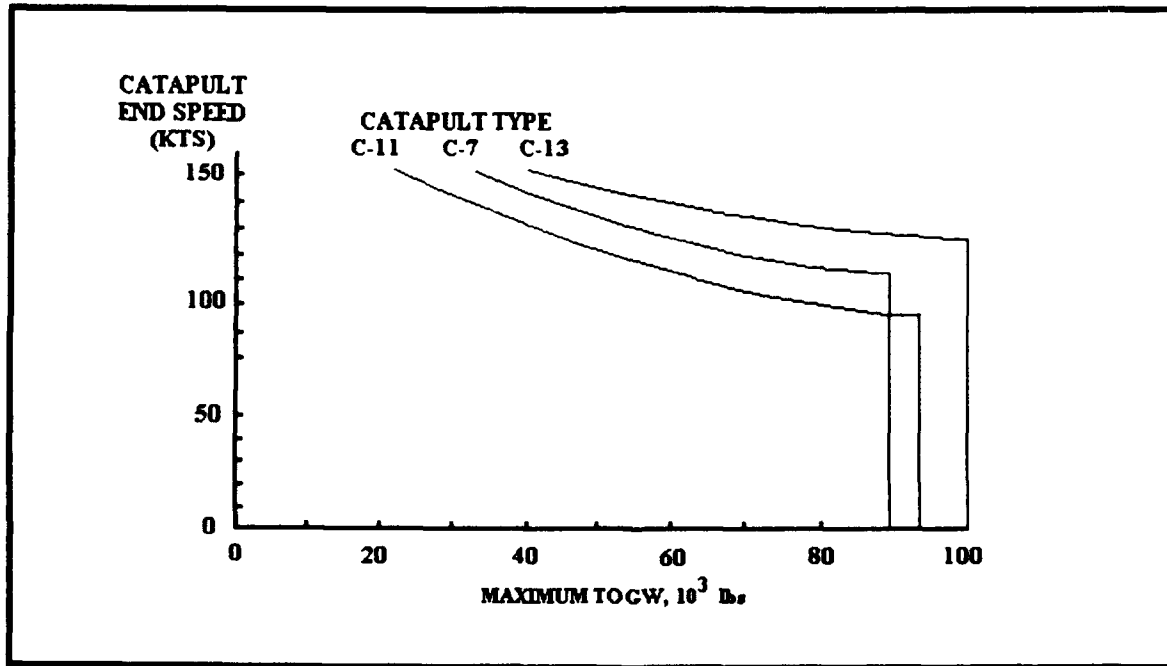


Figure A.1 Catapult End Speeds. From Ref. 10.

## 2. Empty Weight Fraction

Empty-weight fraction is estimated to be 0.5 for initial sizing. This is based on historical trends and also on catapult takeoff and arrested recovery weight limitations. Maximum catapult takeoff weight is approximately 100,000 lbs. From Figure A.2, maximum arrested recovery weight is approximately 50,000 lbs [Ref. 10:p. 92]. These maximums are used as a conservative estimate for initial sizing. The use of advanced

composites in construction of the aircraft could result in a 16% lighter empty weight [Ref. 9:p. 5-2]. This results in an empty weight fraction of:

$$\frac{W_e}{W_0} = \frac{(50,000)(1 - 0.16)}{100,000} = 0.42$$

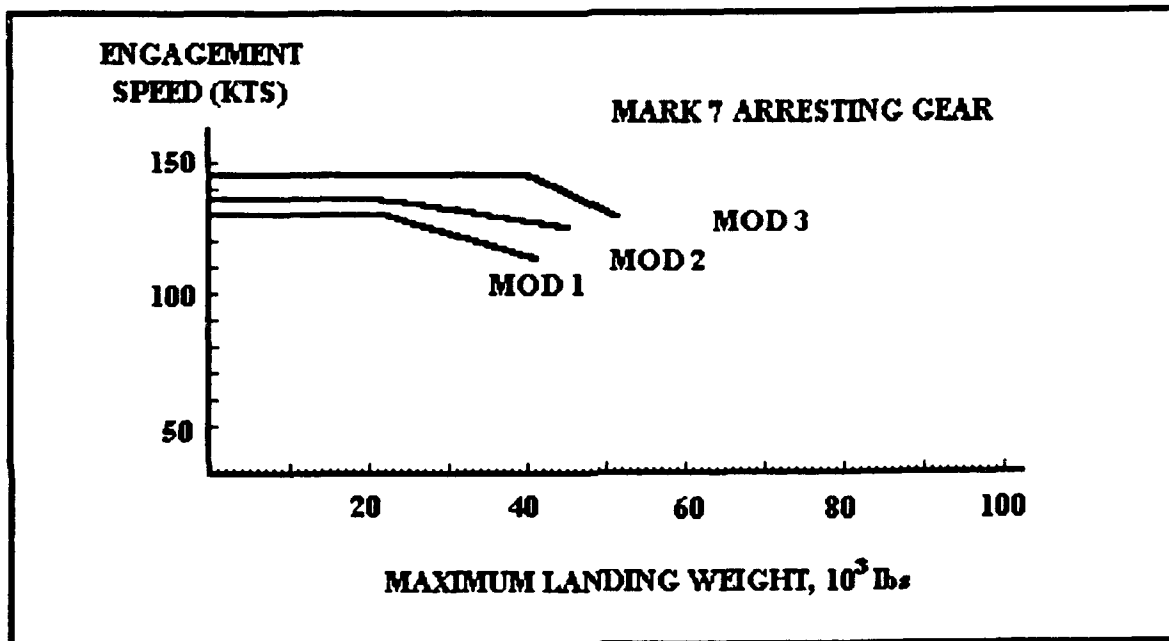


Figure A.2 Arresting Gear Weight Limits. From Ref. 10.

### 3. Mission Segment Weight Fractions

#### a. Warm-up and Takeoff

Weight fraction for engine start, taxi, and takeoff is estimated from historical trends [Ref. 10:p. 104].

$$W_1/W_0 = 0.97$$

**b. Climb and Accelerate**

For supersonic aircraft the climb weight fraction with beginning Mach of 0.1 is approximated by:

$$\frac{W_i}{W_{i-1}} = 0.991 - 0.007M - 0.01M^2$$

where: M = ending Mach number

The beginning Mach number for this design will be based on the catapult end speed for the aircraft weight. From Figure A.1, this is approximately 130 kts or M = .197. For a cruise Mach number of 6.0 the weight fraction for acceleration from M = 0.1 must be divided by the weight fraction for acceleration from M = 0.1 to M = 0.197. [Ref. 10:p. 105]

$$\frac{W_2}{W_1} = \frac{0.991 - 0.007(6.0) - 0.01(36)}{0.991 - 0.007(.197) - 0.01(.039)} = 0.595$$

**c. Cruise**

The Brequet range equation is used for cruise:

$$R = \frac{V}{C} \frac{L}{D} \ln \frac{W_{i-1}}{W_i}$$

This leads to cruise weight fractions of:

$$\frac{W_i}{W_{i-1}} = e^{\frac{-RC}{V(L/D)}}$$

where: R = range

C = specific fuel consumption

V = velocity

L/D = lift-to-drag ratio

(1) Range. Range for each cruise segment (out and back) is 1000 nm.

(2) Specific Fuel Consumption. From Figure A.3, an initial estimate of  $I_{sp}$  equal to 1300 seconds is made for a hydrocarbon-powered scramjet. Specific fuel consumption, the inverse of specific impulse, is equal to  $7.7 \times 10^{-9}/\text{sec}$ .

(3) Velocity. Velocity is calculated assuming a standard atmosphere at 80,000 feet.

$$v = Ma$$

where: M = cruise Mach number

a = speed of sound

At 80,000 feet the speed of sound is 968.08 ft/sec. For a Mach number of 6.0 this gives a velocity of 5808.48 ft/sec.

(4) L/D. L/D is assumed to be 4.0 for initial sizing calculations. This is a conservative assumption based on trends developed during early waverider configurations.

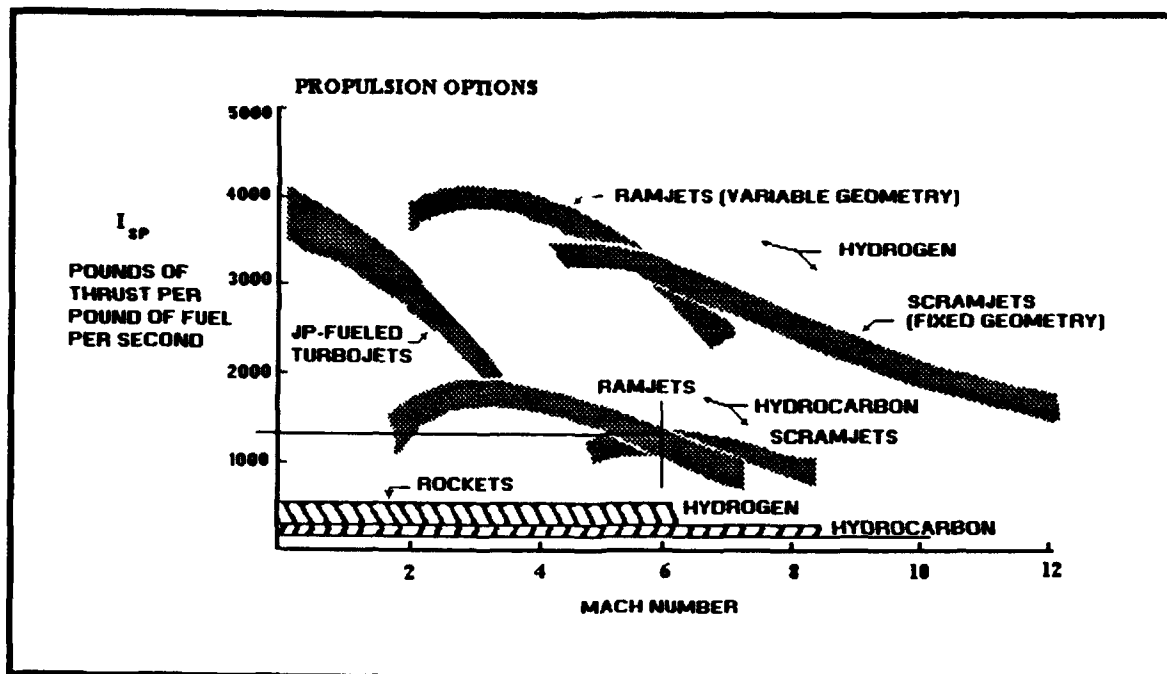


Figure A.3 Specific Impulse Trends.

(5) Cruise Out

$$\frac{W_3}{W_2} = e^{\frac{-(6076000 \text{ ft})(7.7 \times 10^{-4} / \text{sec})}{(5808.48 \text{ ft/sec})(4.0)}} = 0.818$$

(6) Cruise Back

$$\frac{W_5}{W_4} = \frac{W_3}{W_2} = 0.818$$

#### d. Combat

Combat fuel requirements are a function of engine performance and combat duration [Ref. 10:p. 106]. For the specified mission, the combat duration is 20 minutes.

It is assumed for these calculations that combat will be flown at low Mach numbers using the turbojets for propulsion. T/W for this segment is estimated to be 0.5.

$$\frac{W_4}{W_3} = 1 - C(T/W)(d) = 1 - 1.72 \times 10^{-4} (.5)(1200) = 0.897$$

where: C = specific fuel consumption (1/sec)

T/W = combat thrust to weight ratio

d = combat duration (sec)

***e. Loiter***

Typical requirements for aircraft include the capability of 20 minutes of loiter before landing. This allows for such eventualities as missed approaches and fouled runways/decks. Specific fuel consumption for this mission segment is based on the J-58 turbojets and is equal to  $1.72 \times 10^{-4}$ /sec. Loiter for jet-powered aircraft is flown at maximum L/D. Maximum L/D is estimated to be 8.0 for these calculations.

$$\frac{W_6}{W_5} = e^{\frac{-EC}{L/D}} = e^{\frac{-(1200\text{sec})(1.72 \times 10^{-4})}{8.0}} = 0.975$$

where: E = loiter time

***f. Descent for Landing***

Descent for landing is estimated from historical trends [Ref. 10:p. 107].

$$\frac{W_7}{W_6} = 0.990$$



**g. Landing and Taxi Back**

Landing is estimated from historical trends [Ref. 10:p. 107].

$$\frac{W_8}{W_7} = .992$$

**3. Fuel Fraction**

The fuel fraction is calculated from the total mission weight fraction given by the product of the mission segment weight fractions calculated above.

$$\frac{W_8}{W_0} = (.97)(.595)(.818)(.897)(.818)(.975)(.990)(.992) = 0.332$$

$$\frac{W_f}{W_0} = 1.06(1 - 0.332) = 0.708$$

**4. Resulting First Order Estimation of Takeoff Weight**

$$W_0 = W_{crew} + W_{payload} + W_{fuel} + W_{empty}$$

$$= 200 + 400 + (.708)(100,000) + .42(100,000) = 120,600/lbs$$

## APPENDIX B - WAVERIDER CONSTRUCTION

Waveriders are generated in a reverse fashion from most aerodynamic bodies in that the flowfield from which the waverider is derived is known. Waveriders can be generated from the flowfields caused by shapes other than themselves (wedges, cones, etc.) The waveriders of this study were generated from the flowfields caused by axisymmetric circular cones at zero angle of attack. The explanation of waverider construction contained herein will use this type of waverider as an example. The process used for the waveriders of this project is straightforward and fairly standard.

### STEP 1. SOLVE THE FLOWFIELD

The first step in creating a conical flow waverider is to solve for the flowfield generated by a right circular cone of known semi-vertex angle. The Taylor Maccoll equation [Ref. 16:p. 7] is used to generate the solution for this flowfield:

$$(\gamma - 1) / 2 [1 - V_r^2 - (dV_r / d\theta)^2] [2V_r + (dV_r / d\theta) \cot \theta + d^2V_r / d\theta^2 - (dV_r / d\theta) + (dV_r / d\theta)(d^2V_r / d\theta^2)] = 0$$

where:  $V_r$  = nondimensional component of flow velocity along a conical ray

$\theta$  = ray angle from axis

$\gamma$  = ratio of specific heats

### STEP 2. GENERATE FREESTREAM UPPER SURFACE

The generating curve (see Section III) is drawn longitudinally through the cone flowfield to "carve" out the waverider's freestream upper surface. Figure B.1 shows a general cone-derived waverider, the generating cone and the conic shock.

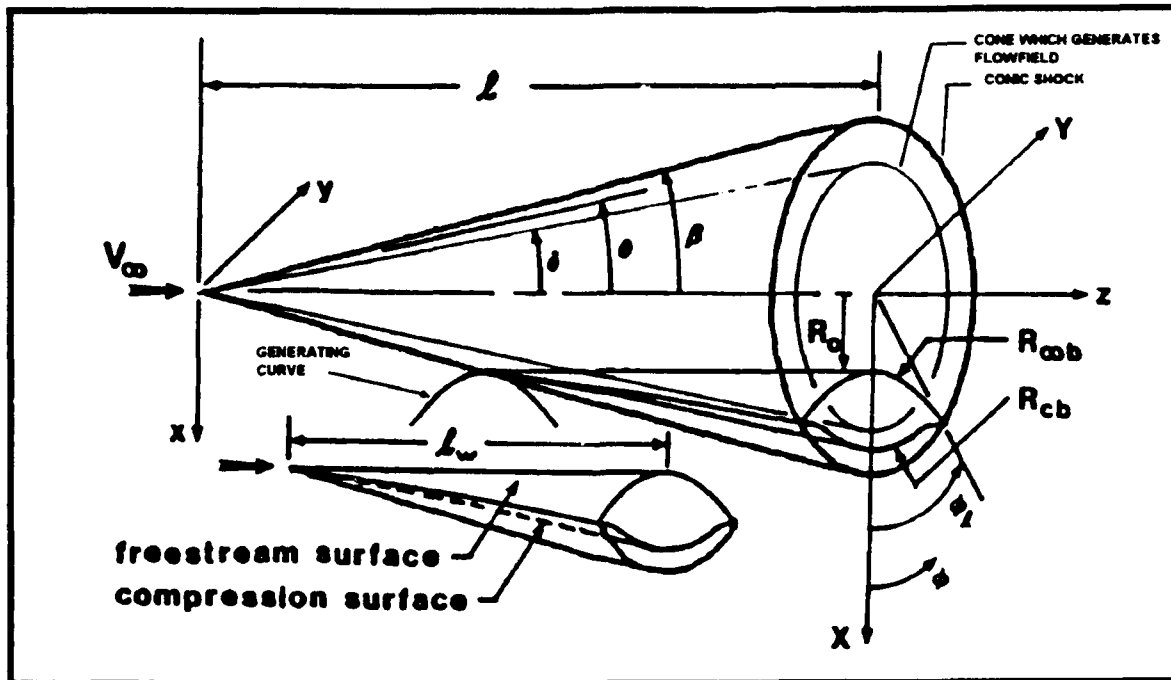


**Figure B.1 Construction of General Cone-Derived Waverider. From Ref. 16.**

### STEP 3. LOWER COMPRESSION SURFACE

Conic streamlines are traced back from the intersection of the shock and the upper surface to generate the lower, compression surface of the waverider.

## APPENDIX C - MODEL SIZING CALCULATIONS

### A. WIND TUNNEL MODEL

The two major factors considered in sizing the wind tunnel model were the test section size and normal force measuring capability of the sting mounted balance. The test section size of the NPS tunnel (32 x 45 inches) limits the span of models to approximately 18 inches. The small size of such a model indicated the need to use a 0.75 inch diameter balance (the smallest available from Ames). The 0.75 inch diameter balances were available with normal force capabilities of 50 and 100 pounds. A general rule of thumb for force measurements is to use approximately 75 percent of the balance capacity at the highest force measured. This will generally result in the best resolution of measured forces. The goal of this sizing analysis was to find the largest model possible which would generate a normal force of 75 percent while at the maximum angle of attack planned for the tests.

The normal force expected in the tunnel is a function of the dynamic pressure,  $q$ , the coefficient of lift,  $C_L$ , and the size of the model. For best resolution, this force should be 37.5 or 75 pounds for the 50 and 100 pound balances, respectively. The maximum angle of attack for the initial tests will be 20 degrees. The predicted  $C_L$  value at 20 degrees angle of attack was calculated by the VORLAX code at NASA Ames as 0.54.

For a standard atmosphere at sea level, the speed of sound is 1116.4 ft/sec and the density is  $2.3769 \times 10^{-3}$  slugs/ft<sup>3</sup>. The planned test velocity is 140 kts or 236.3 ft/sec. From this, the dynamic pressure is calculated as follows:

$$q = \frac{1}{2} \rho v^2 = (.5)(2.3769 \times 10^{-3})(236.3)^2 = 66.36 \text{ lbs / ft}^2$$

where:  $\rho$  = density (slugs/ft<sup>3</sup>)

$v$  = velocity (ft/sec)

From the optimized hydrocarbon-powered configuration, the plan area,  $s$ , is given by:

$$s = (.674)(l)^2(.9416)$$

The lift force can be calculated by:

$$L = C_L q s$$

where:  $C_L$  = coefficient of lift

$q$  = dynamic pressure

$s$  = plan area

The 100 pound balance was ruled out due to the inability of an 18 inch model (the largest possible in the tunnel) to generate 75 pounds of normal force (lift) at 20 degrees angle of attack as shown below:

$$L = (.54)(66.36)(1.428) = 51.2 \text{ lbs}$$

The model length necessary to generate 37.5 pounds of force can be found in a reverse fashion:

$$l = \sqrt{\frac{37.5}{(.54)(66.36)(.674)(.9416)}} = 1.28 \text{ ft} = 15.4 \text{ in}$$

## B. WATER TUNNEL MODEL

The major factor in sizing the water tunnel model is flow blockage by the model in the water tunnel test section. A general rule of thumb is to limit this flow blockage to five percent of the test section area. The test section area of the NPS water tunnel facility is  $300 \text{ in}^2$ . This gives a desired maximum blockage of  $15 \text{ in}^2$ . The blockage is a function of the model length and angle of attack. For this series of tests the maximum angle of attack of interest is approximately 20 degrees. The maximum length of the model can be calculated by knowing the plan area which generates the maximum blockage at 20 degrees angle of attack and is calculated below.

The maximum blockage is given by:

$$(.05)(300 \text{ in}^2) = 15 \text{ in}^2$$

From this, the plan area of the model follows as:

$$\frac{15 \text{ in}^2}{\sin(20^\circ)} = 43.86 \text{ in}^2$$

The relations between length, span and plan area are known from the optimized hydrocarbon-powered configuration and are:

$$\text{plan area} = (.674)(\text{length})(\text{span})$$

$$\text{span} = (.9416)(\text{length})$$

From this, the model length is computed as:

$$\text{length} = \sqrt{\frac{43.857}{(.674)(.9416)}} = 8.3 \text{ in}$$

From the results above, a length of eight inches was selected. This length will result in a maximum angle of attack of approximately 22 degrees at five percent flow blockage.

## REFERENCE LIST

1. Kuchemann, D., *The Aerodynamic Design of Aircraft*, Pergamon Press, 1978.
2. Tincher, D. J., "Application of Viscous-Optimized Waverider Technology for Evader MaRV and HGV Missions," *Proceedings of 1st Hypersonic Waverider Symposium*, October 1990.
3. Louis, M. J., Kothari, A. P., "Hypersonic Waveriders for Planetary Maneuvering," *Proceedings of 1st Hypersonic Waverider Symposium*, October 1990.
4. Nonweiler, T.R.F., "Aerodynamic Problems of Manned Space Vehicles", *Journal of the Royal Aeronautical Society*, v. 63, pp. 521-528.
5. Seddon, J., and Spence, A., "The Use of Known Flow Fields as an Approach to the Design of High Speed Aircraft", *Hypersonic Boundary Layers and Flow Fields*, AGARD CP No. 30, 1968.
6. Eggers, A. J., and others, "Hypersonic Waverider Configurations from the 1950's to the 1990's," *Proceedings of 1st Hypersonic Waverider Symposium*, October 1990.
7. Schindel, L., "Limitations of Waveriders," *Proceedings of 1st Hypersonic Waverider Symposium*, October 1990.
8. Vanhoy, D. L., *Low-Speed Wind Tunnel Testing of a Mach 6 Viscous Optimized Waverider*, Master's Thesis, University of Maryland, College Park, Maryland, May 1988.
9. Nicolai, L. M., *Fundamentals of Aircraft Design*, METS, Inc., 1984.
10. Raymer, D. P., *Aircraft Design: A Conceptual Approach*, American Institute of Aeronautics and Astronautics, 1992.
11. Vanderplaats, G. N., and Hansen, S. R., *DOT Users Manual*, Version 2.04B, VMA Engineering, 1990.
12. Richardson, D., *The Illustrated Encyclopedia of Modern Warplanes*, Crescent Books, 1982.
13. Perkins, H. C., *Air Pollution*, McGraw-Hill, 1974.
14. Anderson, J. D., *Modern Compressible Flow With Historical Perspective*, McGraw-Hill, 1990.



15. Pessin, D. N., *Aerodynamic Analysis of Hypersonic Waverider Aircraft*, Master's Thesis, Cal Poly State University, San Luis Obispo, California, April 1993.
16. Anderson, J. D., Lewis, M. J., and Corda, S., "Several Families of Viscous Optimized Waveriders—A Review of Waverider Research at the University of Maryland," *Proceedings of 1st Hypersonic Waverider Symposium*, October 1990.
17. Anderson, J. D., *Introduction to Flight*, McGraw-Hill, 1978.
18. Pope, A., and Harper, J. J., *Low-Speed Wind Tunnel Testing*, John Wiley & Sons, Inc, 1966.
19. Rasmussen, M. L., and Xiaohai, H., "Analysis of Cone-Derived Waveriders by Hypersonic Small-Disturbance Theory," *Proceedings of 1st Hypersonic Waverider Symposium*, October 1990.
20. Hebbar, S., and Sommers, J., "Wind Tunnel Studies of Support Strut Interferences on a 3g YF-17 Fighter Aircraft Model at High Angles-of-Attack," paper presented at the AIAA 8th Applied Aerodynamics Conference, Portland, Oregon, 20-22 August 1990.
21. Hebbar, S., Platzer, M., and Cavazos, O., "A Water Tunnel Investigation of the Effects of Pitch Rate and Yaw on Lex Generated Vortices of a F/A-18 Fighter Aircraft Model," paper presented at the 29th Aerospace Sciences Meeting, Reno, Nevada, 7-10 January 1991.
22. Agrawal, B., *Design of Geosynchronous Spacecraft*, Englewood Cliffs: Prentice-Hall, 1986.

### INITIAL DISTRIBUTION LIST

- |    |  |   |
|----|--|---|
| 1. | Defense Technical Information Center<br>Cameron Station<br>Alexandria, Virginia 22304-6145                                   | 2 |
| 2. | Library, Code 0142<br>Naval Postgraduate School<br>Monterey, California 93943-5002   | 2 |
| 3. | Professor C. F. Newberry<br>Dept. of Aeronautics and Astronautics<br>Naval Postgraduate School<br>Monterey, California 93943 | 5 |
| 4. | Professor D. J. Collins<br>Dept. of Aeronautics and Astronautics<br>Naval Postgraduate School<br>Monterey, California 93943  | 1 |
| 5. | Mr. J. V. Bowles<br>Systems Analysis Branch<br>NASA Ames Research Center<br>Moffett Field, California 94035                  | 5 |
| 6. | Mr. George Kidwell<br>Systems Analysis Branch<br>NASA Ames Research Center<br>Moffett Field, California 94035                | 1 |